Principles of electrowetting with two immiscible electrolytic solutions

2006 J. Phys.: Condens. Matter 18 2837

(http://iopscience.iop.org/0953-8984/18/10/009)

INSTITUTE OF PHYSICS PUBLISHING JOURNAL OF PHYSICS: CONDENSED MATTER

J. Phys.: Condens. Matter **18** (2006) 2837–2869 doi:10.1088/0953-8984/18/10/009

Principles of electrowetting with two immiscible electrolytic solutions

C W Monroe[1], L I Daikhin[2], M Urbakh[2] and A A Kornyshev[1]

[1] Department of Chemistry, Imperial College, London SW72AZ, UK
[2] School of Chemistry, Tel Aviv University, Ramat Aviv, 69978, Israel

E-mail: cwmonroe@ic.ac.uk and a.kornyshev@ic.ac.uk

Received 11 November 2005, in final form 9 December 2005
Published 20 February 2006
Online at stacks.iop.org/JPhysCM/18/2837

Abstract

This paper gives a theoretical background for a new electrowetting system based on interfaces between two immiscible electrolytic solutions. It presents a linear-response Poisson–Boltzmann theory to describe an electrolytic droplet on a charged flat electrode, bounded by another electrolytic solution. Immiscibility of the two solutions causes back-to-back double layers to form at the liquid–liquid interface, which dramatically change the polarization response. Useful approximations are developed that apply to droplets with typical experimental volumes. Under the derived approximations, minimization of the free-energy functional proves that polarized droplets take the shape of truncated spheres and reveals a law of contact-angle variation with applied potential. This dependence is determined by the interfacial tensions and the electrolyte concentrations in and dielectric constants of the liquid phases. The study of contact-angle variation with electrode potential may be used, among other applications, as a new tool to investigate the effect of solution properties on liquid–liquid surface tensions.

(Some figures in this article are in colour only in the electronic version)

1. Introduction

In microfluidic technologies, electrowetting is a popular means by which to regulate small quantities of liquid. 'Lab-on-a-chip' devices for biomedical diagnostics are perhaps the best studied area of microfluidics, but electrowetting is useful in a far broader range of miniaturized systems. Much recent research of electrowetting has focused on the precise manipulation of isolated droplets on polarized surfaces for optical technologies. Potential applications of liquid-droplet electrowetting include variable-focus lens technology [1, 2], electronic displays [3, 4], fibre optics [5, 6], and microelectromechanical devices [7, 8].

Below, we study the polarization response of a new three-phase electrowetting system. It consists of a liquid droplet, which lies on the surface of a flat solid electrode and is surrounded by another liquid. The two liquids are immiscible. In experiments, the droplet is typically an oil, and the surrounding liquid is water—but in principle this situation could be reversed. A certain amount of electrolyte is dissolved in each of the two liquid phases: the oil contains a fatty salt, preferentially soluble in nonpolar organic liquids (e.g. tetrabutylammonium tetraphenylborate), whereas the water contains a typical inorganic buffer electrolyte. The free energies of transfer of the organic electrolyte into water and the inorganic electrolyte into oil are large enough to prevent permeation of the electrolytes into their neighbouring phases.

Under polarization, the immiscibility of the two solutions causes back-to-back electrical double layers to form at the liquid–liquid interface. Interfaces of this kind are called ITIES (interfaces between two immiscible electrolytic solutions); they have been thoroughly studied in two-phase geometries [9–17]. Common applications of the ITIES include phase-transfer catalysis, sensor technology, and biomimetic and molecular devices.

Studies of ITIES in three-phase solid–liquid–liquid geometries are still in their infancy [18–20]. Properties of the triple electrowetting system, including the potential distribution, the potential dependence of the three-phase contact angle, and the dynamics of charge transfer, are not well understood. This article provides a first theoretical analysis of this potentially useful configuration.

In typical experiments the electrolyte concentrations and droplet volume are fixed. When a potential is applied to the system, the salt in the droplet does not escape, no matter how the shape of the liquid–liquid interface changes. Because no reaction consumes either of the liquids, the total volume of the droplet also remains constant with potential. Thus, the average electrolyte concentration in the droplet remains unchanged as its shape changes with polarization.

Our main task is to find the shape of the droplet for a given potential drop between the working and counter electrodes, and, specifically, the contact angle between the liquid–liquid interface and the working electrode. To implement this task requires an understanding of the potential distribution in this system as a function of the applied potential, which is also relevant to future analysis of kinetic processes in the three-phase system. Problems of this type are familiar from the theory of electrowetting [21–24]. The essential new element in our study is the ion-impermeable liquid–liquid interface; this makes the physics very different from that employed in the papers cited above.

A natural approach to this problem is as follows. Solve the Poisson–Boltzmann (PB) equations—applicable at moderate polarizations and electrolyte concentrations—to determine the potential distributions in the two liquid phases for a droplet of a given volume but an arbitrary shape. Use the potential distributions to evaluate the electrostatic energy, which can be added to the surface energy to give the total free energy. Finally, minimize the free-energy functional with ionic numbers fixed in the droplet to determine the shape, and, thereby, obtain the contact angle. The conservation of ionic numbers in the droplet is a key feature of this system which must be taken into account.

Mathematically, this approach is difficult. Therefore to understand the basic physics, we consider small electrode polarizations, for which the PB equations can be linearized. A nonlinear version of the theory will be reported elsewhere.

To elucidate the physics of polarized immiscible-electrolytic droplets, the paper first provides an electrostatic analysis of droplets with fixed shapes. This discussion explains two useful and general approximations that apply to the system. To a certain extent, at least for large droplets (with mean radius of curvature $\gg 10^3$ Debye lengths in the droplet phase), we

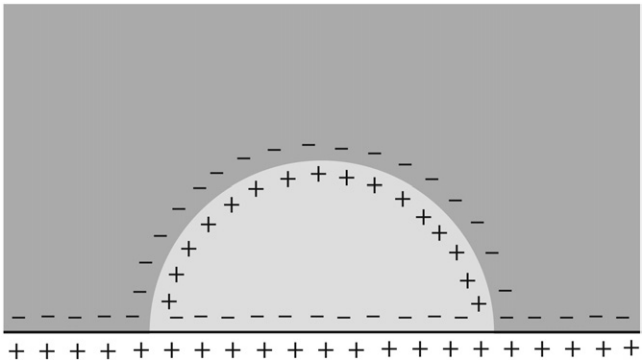

Figure 1. Sketch of the charge distribution when the net charge is conserved in an electrolytic droplet.

show that the electrostatic analysis of a two-electrolyte system actually becomes much simpler than that of a system with pure dielectric liquids.

First, a hemispherical droplet is treated; in this case, an exact solution of the PB equations can be obtained. The results show that droplets with volumes typically used in experiments may be described as 'infinitely large'—the upshot being that most of the liquid–liquid interface resides at a constant potential. Second, droplets that take the shape of truncated spheres are analysed in the large-volume regime. It is shown that the electric field components diverge near the line of three-phase contact, but that the divergence does not significantly affect the total electrostatic energy. This remains true at all contact angles of the truncated sphere.

After this preliminary analysis, the fixed-shape restriction is relaxed and the method described above is employed: the free energy is used directly to determine the droplet shape and contact angle. Minimization of the free-energy functional proves that the optimal shape for an immiscible-electrolytic droplet at macroscopic length scales is indeed a truncated sphere.

The ultimate result is a simple formula, equation (61), which shows how the contact angle varies with applied potential. It is expressed in terms of the dielectric properties of the solvents, the Debye lengths of the electrolytes, the contact angle at zero polarization, and the liquid–liquid surface tension. For solutions with given composition, this formula can easily be used to determine liquid–liquid surface tensions from experimental measurements of the contact angle as a function of potential.

2. Consequences of ion-number conservation in a droplet

To envision what happens to the immiscible-electrolytic droplet when the electrode is polarized, perform a thought experiment. Imagine that the electrode is raised to a positive potential. One expects a response like that shown in figure 1. Within the droplet, negative charges are driven to aggregate near the charged electrode surface. Because the numbers of each type of ion within it are fixed, the interior of the droplet cannot carry a net charge. When anions in the droplet are drawn toward the electrode, a net excess of cations must arise elsewhere because the droplet surface is impermeable. The excess positive ions may be expected to move towards the liquid–liquid interface, where they can be balanced by negative ions from the surroundings.

This constraint on the interior of the droplet is expressed through two equations that require the conservation of the individual ionic numbers within it. Multiplying these two equations by the ionic equivalent charges and adding them gives a single equation that expresses the

conservation of the net droplet charge, through the integral

$$\int_{V_\mathrm{d}} \left(z_+^\mathrm{d} c_+^\mathrm{d} + z_-^\mathrm{d} c_-^\mathrm{d}\right) \mathrm{d}V = 0. \tag{1}$$

Here V_d is the droplet volume; c_i^d and z_i^d are the concentration and equivalent charge of ion i in the droplet, respectively. A consistent physical formulation must account for this additional restriction.[3]

The PB equations in the droplet interior must be written with care to take into account that its boundaries inhibit the free thermal motion of ions. As a result of this entropic limitation, the droplet resides at a potential with a magnitude elevated from that of the surrounding solution far from the electrode. In other words, the potential at which charge density is zero in the droplet, denoted by Φ^*, is shifted towards the electrode potential from the potential in the outer liquid bulk. One can account for the potential shift due to constrained ion motion by taking the distributions of concentrations to be

$$c_i^\mathrm{d} = c_0^\mathrm{d} \nu_i^\mathrm{d} \exp\left[-\frac{z_i^\mathrm{d} F\left(\Phi_\mathrm{d} - \Phi^*\right)}{RT}\right], \tag{2}$$

where Φ_d, c_0^d, and ν_i^d are the potential, bulk electrolyte concentration, and stoichiometric number of ion i in the droplet, respectively; F is Faraday's constant, R is the gas constant, and T is the absolute temperature. Because Φ_d and Φ^* have the same sign, equation (2) expresses that it is more difficult to induce local concentration changes in the droplet because the ions within it are not fully free to move. Linearization of the concentration distributions in equation (2) near Φ^* yields an equation on electrostatic potential in the droplet,

$$\nabla^2\left(\Phi_\mathrm{d} - \Phi^*\right) = \frac{\Phi_\mathrm{d} - \Phi^*}{\lambda_\mathrm{d}^2}, \tag{3}$$

where λ_d is the Debye length in the droplet phase. Ultimately, Φ^* is found by substitution of the solution of this equation into equation (1). The potential in the bulk of the outer solution is zero; it provides an infinite source of ions and does not inhibit their free motion. The PB equation that describes the surroundings uses standard Boltzmann distributions linearized around null potential, yielding

$$\nabla^2 \Phi_\mathrm{s} = \frac{\Phi_\mathrm{s}}{\lambda_\mathrm{s}^2}, \tag{4}$$

where Φ_s is the potential in the outer solution and λ_s is its Debye length. The equation

$$\lambda_j = \sqrt{\frac{\epsilon_0 \epsilon_j RT}{F^2 c_0^j \left(z_+^{j\,2} \nu_+^j + z_-^{j\,2} \nu_-^j\right)}}; \qquad j = \mathrm{s}, \mathrm{d}, \tag{5}$$

in which ϵ_0 is the permittivity of free space and ϵ_j is the dielectric constant of phase j, gives the Debye length. The Debye length retains this familiar definition in both phases.

[3] Equation (1) is a looser constraint than the two equations on the ion numbers. When a droplet is very small, the concentration prefactor c_0^d in the Boltzmann distributions may differ from the average electrolyte concentration, $c_\mathrm{ave}^\mathrm{d}$. In these cases c_0^d can be lowered appreciably from $c_\mathrm{ave}^\mathrm{d}$; as ions are drawn toward the interfaces in the droplet interior, the concentration is depleted at points where the local charge density is zero. For symmetric electrolytes, $c_0^\mathrm{d} \approx c_\mathrm{ave}^\mathrm{d}$ when the applied potential obeys

$$|\Phi_0| \ll \frac{4RT}{F z_+^\mathrm{d}} \sqrt{\frac{r_\mathrm{d}}{\lambda_\mathrm{d}}},$$

where λ_d is the droplet-phase Debye length given by equation (5), computed with the average concentration. This constraint on potential is less strict than the approximation that justifies linearization of the PB equations when the droplet's radius of curvature r_d exceeds $\sim 50\lambda_\mathrm{d}$.

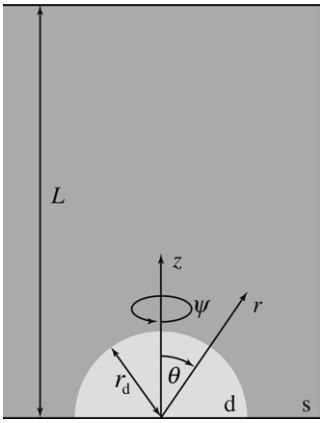

Figure 2. Sketch of the experimental geometry.

3. Electrostatics of hemispherical droplets

To elucidate the physical impact of ion-number conservation in the electrowetting of immiscible-electrolytic solutions, we first explore the electrostatics with idealized droplets of fixed shape. The most easily tractable case is a hemispherical droplet, for which exact solutions to the linearized PB equations can be obtained. This section provides the potential and charge distributions for polarized hemispherical droplets in three regimes of size, and determines the ranges of droplet radius over which each asymptotic result is most accurate.

3.1. Coordinate system and parameters

A hemispherical droplet is taken to lie between two parallel planar electrodes separated by distance L, as shown in figure 2. The electrode on which the droplet sits is assumed to be an ideal conductor, and thus is an isopotential surface at potential Φ_0. The droplet has a radius of curvature r_d. Let z designate the distance perpendicular to the near electrode through the axis of symmetry. We assume the interelectrode distance $L \gg r_d$, making the system semi-infinite with $\Phi \to 0$ as $z \to \infty$. Designate the phase within the droplet by d and the surrounding phase by s, and the corresponding potentials by Φ_d and Φ_s. In spherical coordinates, this system is insensitive to the azimuthal angle ψ because it is rotationally symmetric about the z-axis; the potential in phase j, Φ_j, depends on the radial coordinate r and polar angle θ.

To simplify notation in the governing equations and boundary conditions, introduce the dimensionless radial coordinate, ξ, and size of the droplet, δ,

$$\xi = \frac{r}{\sqrt{\lambda_d \lambda_s}}, \qquad \delta = \frac{r_d}{\sqrt{\lambda_d \lambda_s}}, \qquad \text{and} \qquad x = \cos\theta, \tag{6}$$

and transform the polar components of the governing equations to a quasi-Cartesian variable, x, that ranges from 0 to 1. The potentials are nondimensionalized by

$$\phi_j = \frac{\Phi_j}{\Phi_0} \qquad \text{and} \qquad \phi^* = \frac{\Phi^*}{\Phi_0}. \tag{7}$$

In this way, they are scaled to be between 1 at the electrode and 0 far away. Two additional parameters characterize the physical properties of the immiscible solutions,

$$\chi = \sqrt{\frac{\epsilon_s}{\epsilon_d}}, \qquad \zeta = \sqrt{\frac{\lambda_s}{\lambda_d}}. \tag{8}$$

The relative dielectric properties are expressed through χ, and the properties of the two electrolytes through ζ.

In a discussion of relevant quantities, variables associated with the distribution of charges should also be addressed. According to the Boltzmann distribution, equation (2), the local charge density in phase j, ρ_e^j, is given by

$$\rho_e^d = -\frac{\epsilon_0\epsilon_d\Phi_0}{\lambda_d^2}\left(\phi_d - \phi^*\right) \qquad \text{and} \qquad \rho_e^s = -\frac{\epsilon_0\epsilon_s\Phi_0}{\lambda_s^2}\phi_s. \tag{9}$$

A dimensionless charge density, P_e^j, with minimum -1 at the near electrode in the solution surrounding the droplet, can be defined as

$$P_e^j = \frac{\lambda_s^2}{\epsilon_0\epsilon_s\Phi_0}\rho_e^j. \tag{10}$$

In terms of this quantity, equations (9) become

$$P_e^d = -\frac{c_0^d\left(z_+^{d\,2}\nu_+^d + z_-^{d\,2}\nu_-^d\right)}{c_0^s\left(z_+^{s\,2}\nu_+^s + z_-^{s\,2}\nu_-^s\right)}\left(\phi_d - \phi^*\right) \qquad \text{and} \qquad P_e^s = -\phi_s. \tag{11}$$

When the two electrolyte concentrations are the same and the electrolytes are symmetric with the same equivalent charge, the prefactor on ϕ_d is equal to unity in P_e^d.

3.2. Governing equations

The potential distribution around a hemispherical droplet at small applied potentials is given by the dimensionless forms of equations (3) and (4) in spherical coordinates,

$$\begin{aligned}
&\frac{\partial}{\partial\xi}\left(\xi^2\frac{\partial\phi_d}{\partial\xi}\right) + \left[(1-x^2)\frac{\partial^2\phi_d}{\partial x^2} - 2x\frac{\partial\phi_d}{\partial x}\right] = \xi^2\zeta^2\left(\phi_d - \phi^*\right), \qquad 0 \leqslant \xi \leqslant \delta,\\
&\frac{\partial}{\partial\xi}\left(\xi^2\frac{\partial\phi_s}{\partial\xi}\right) + \left[(1-x^2)\frac{\partial^2\phi_s}{\partial x^2} - 2x\frac{\partial\phi_s}{\partial x}\right] = \frac{\xi^2\phi_s}{\zeta^2}, \qquad \xi \geqslant \delta.
\end{aligned} \tag{12}$$

This system takes the boundary conditions

$$\phi_d(\xi, 0) = 1 \qquad \text{and} \qquad \phi_s(\xi, 0) = 1, \tag{13}$$

$$\phi_d(0, x) = \text{finite} \qquad \text{and} \qquad \lim_{\xi\to\infty}\phi_s(\xi, x) = 0. \tag{14}$$

The electric displacements are matched at the liquid–liquid interface by

$$\frac{1}{\chi}\left.\frac{\partial\phi_d}{\partial\xi}\right|_{(\delta,x)} = \chi\left.\frac{\partial\phi_s}{\partial\xi}\right|_{(\delta,x)}, \tag{15}$$

whereas the potential-matching condition is

$$\phi_d(\delta, x) = \phi_s(\delta, x). \tag{16}$$

Inside the droplet, the charge distribution linearized around Φ^* (equation (9)) reduces equation (1) to

$$\int_0^1\left[\int_0^\delta\left(\phi_d - \phi^*\right)\xi^2\,d\xi\right]dx = 0. \tag{17}$$

Once a potential distribution has been obtained to satisfy equations (12)–(16), this last equation specifies the value of ϕ^*.

3.3. General solution for hemispherical droplets

The governing system is separable and may be solved with Fourier–Legendre series,

$$\phi_{\mathrm{d}} - \phi^* = \left(1 - \phi^*\right) \mathrm{e}^{-\xi x \zeta} + \sum_{m=0}^{\infty} d_m \left[\sqrt{\frac{\delta}{\xi}} \frac{I_{2m+\frac{3}{2}}(\xi\zeta)}{I_{2m+\frac{3}{2}}(\delta\zeta)} \right] P_{2m+1}(x),$$

$$\phi_{\mathrm{s}} = \mathrm{e}^{-\xi x/\zeta} + \sum_{m=0}^{\infty} s_m \left[\sqrt{\frac{\delta}{\xi}} \frac{K_{2m+\frac{3}{2}}(\xi/\zeta)}{K_{2m+\frac{3}{2}}(\delta/\zeta)} \right] P_{2m+1}(x). \tag{18}$$

In the sums, d_m and s_m are Fourier–Legendre coefficients; $I_{2m+\frac{3}{2}}$ and $K_{2m+\frac{3}{2}}$ are modified Bessel functions of the first and third kind, respectively, at order $2m + \frac{3}{2}$. Orthogonality properties of the odd Legendre polynomials, P_{2m+1}, can be used to obtain d_m and s_m to satisfy the matching conditions. The Sturm–Liouville theorem guarantees that both sums converge.

After insertion of the two Fourier–Legendre series and use of the orthogonality properties, boundary conditions (15) and (16) yield two equations to determine d_m and s_m. These can be expressed concisely in the matrix notation. Define the matrix $\mathbf{C}_m$ as

$$\mathbf{C}_m = \begin{bmatrix} -1 & 1 \\ \dfrac{\zeta I_{2m+\frac{5}{2}}(\delta\zeta)}{\chi I_{2m+\frac{3}{2}}(\delta\zeta)} + \dfrac{2m+1}{\delta\chi} & \dfrac{\chi K_{2m+\frac{1}{2}}(\delta/\zeta)}{\zeta K_{2m+\frac{3}{2}}(\delta/\zeta)} + \dfrac{2\chi(m+1)}{\delta} \end{bmatrix}, \tag{19}$$

and column vectors $\mathbf{f}_m$ and $\mathbf{g}_m$ by

$$\mathbf{f}_m = \begin{bmatrix} \int_0^1 \left(\mathrm{e}^{-x\delta\zeta} - \mathrm{e}^{-x\delta/\zeta}\right) P_{2m+1}(x)\,\mathrm{d}x \\ \int_0^1 x \left(\frac{\zeta}{\chi}\mathrm{e}^{-x\delta\zeta} - \frac{\chi}{\zeta}\mathrm{e}^{-x\delta/\zeta}\right) P_{2m+1}(x)\,\mathrm{d}x \end{bmatrix}, \tag{20}$$

$$\mathbf{g}_m = \begin{bmatrix} \int_0^1 \left(1 - \mathrm{e}^{-x\delta/\zeta}\right) P_{2m+1}(x)\,\mathrm{d}x \\ -\frac{\zeta}{\chi}\int_0^1 x\mathrm{e}^{-x\delta\zeta} P_{2m+1}(x)\,\mathrm{d}x \end{bmatrix}. \tag{21}$$

The Fourier–Legendre coefficients are given by the matrix equation

$$\begin{bmatrix} d_m \\ s_m \end{bmatrix} = (4m+3)\,\mathbf{C}_m^{-1}\mathbf{f}_m + \phi^*(4m+3)\,\mathbf{C}_m^{-1}\mathbf{g}_m. \tag{22}$$

These coefficients account for the liquid–liquid interface: in equation (22), $\mathbf{f}_m$ is the contribution of electrostatics without ion conservation (when $\phi^* = 0$); $\mathbf{g}_m$ accounts for the conservation of ionic masses (i.e., for ions reflected from the impermeable interface).

The integral from the charge-conservation condition, equation (17), also needs to be evaluated. To simplify notation in the condition, introduce the function h_m,

$$h_m = \frac{\zeta^3\sqrt{\delta}}{I_{2m+\frac{3}{2}}(\delta\zeta)} \left[\int_0^{\delta} \xi^{\frac{3}{2}} I_{2m+\frac{3}{2}}(\xi\zeta)\,\mathrm{d}\xi\right] \left[\int_0^1 P_{2m+1}(x)\,\mathrm{d}x\right]. \tag{23}$$

Then the consistency relation for charge conservation becomes

$$\left(1 - \phi^*\right)\left[\tfrac{1}{2}(\delta\zeta)^2 - 1 + (1+\delta\zeta)\,\mathrm{e}^{-\delta\zeta}\right] + \sum_{m=0}^{\infty} d_m h_m = 0. \tag{24}$$

This is an equation on ϕ^*. As d_m depends on ϕ^*, this equation must be solved with Newton–Raphson iteration. For details regarding computation of the integrals in $\mathbf{f}_m$, $\mathbf{g}_m$, and h_m when the droplet is small, see appendix A.

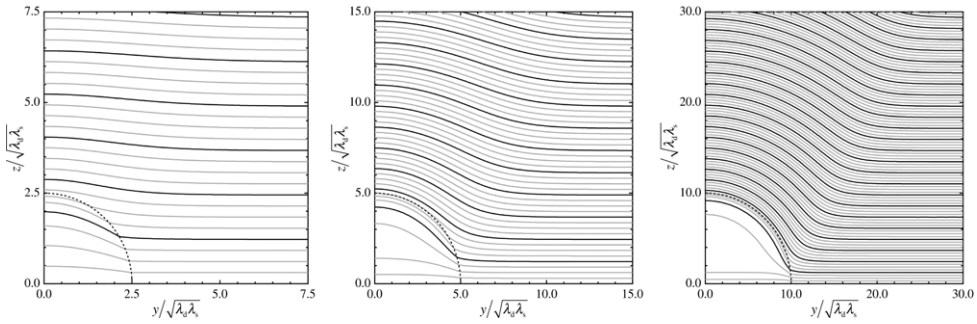

Figure 3. A potential plateau forms as the droplet radius increases. Contour plots of $\ln\phi$ as a function of position in Cartesian coordinates for (from left to right) $\delta = 2.5$, 5, and 10. The contour lines are at intervals of -0.25 in $\ln\phi$; dark lines show negative integer values, and the electrode is fixed at $\ln\phi = 0$. The droplet surface is shown as a dotted line.

Table 1. Properties of the water/nitrobenzene (NB) ITIES used to generate figures. Dielectric constants are taken to be those of the pure solvents [11, 25].

Phase d (nitrobenzene)		Phase s (water)	
ϵ_d	34.82	ϵ_s	78.33
c_0^d	0.01 M	c_0^s	0.01 M
λ_d	2.03 nm	λ_s	3.04 nm
Dimensionless parameters			
χ		1.500	
ζ		1.225	

3.4. Small hemispherical droplet results

Table 1 shows the parameters used to compute distributions for three test cases with 'nanodroplets' of various radii of the order of the droplet-phase Debye length. In the test cases, $\delta = 2.5$, 5, and 10. We consider the case when the droplet is a 0.01 M solution in nitrobenzene, and the surrounding aqueous solution is also 0.01 M. Both electrolytes are taken to be 1:1.

To generate figures 3–6, 80 terms were kept in the Fourier–Legendre series, yielding numerical results accurate to the fifth significant digit. For the $\delta = 2.5$, 5, and 10 cases, $\phi^* = 0.6045$, 0.5345, and 0.4962, respectively.

Potential and charge distributions for the three cases are shown in figures 3 and 4. One can see from the potential distributions that as δ increases, a plateau of potential near ϕ^* arises within the droplet; the charge-density distributions are similar to the qualitative distribution sketched in figure 1. Appendix B provides a discussion that contrasts these results with the situation in which the interface is permeable.

Figure 5 presents the potential along the liquid–liquid surface. It shows that as δ increases, much of the liquid boundary begins to retain a constant potential; the extent of this isopotential region increases with droplet size. Figure 6 shows the normal electric displacement and tangential field at the interface versus θ. The slopes of both increase in magnitude with δ near the contact line, $\theta = \pi/2$. Both components of the field become nearly constant across the liquid boundary when the droplet radius rises: the normal displacement reaches a constant and the tangential field vanishes.

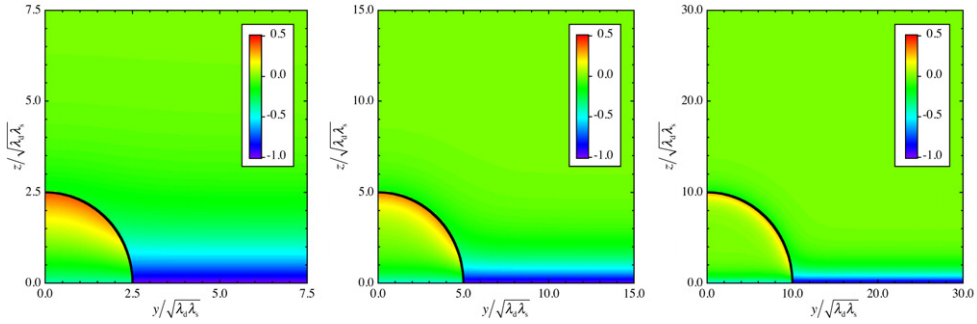

Figure 4. Charges condense near all three interfaces. Charge distributions for (from left to right) droplets with $\delta = 2.5$, 5, and 10. The droplet surface is shown as a solid line in each figure, and the legend sets a correspondence between the colours on the map and the values of the dimensionless charge density, P_e^j.

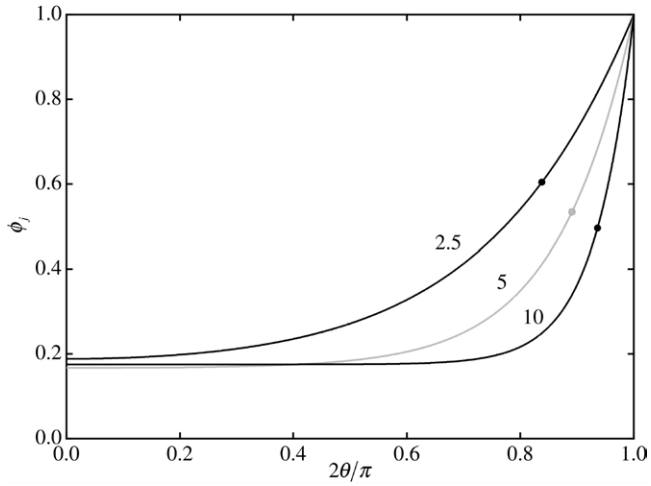

Figure 5. The interfacial potential becomes constant over most of the surface as the droplet radius increases. Potential along the liquid–liquid interface, $\phi_\mathrm{s} = \phi_\mathrm{d} = \phi_j$, as a function of polar angle for $\delta = 2.5$, 5, and 10. A solid circle on each curve marks the angle at which the charge density is zero on the droplet side of the surface.

3.5. Large droplets

Although an analysis of 'nanodroplets' has yielded some insight toward the distributions of charge and potential, in experiments droplets are most often of macroscopic dimensions (a volume $>1\ \mu$l, corresponding to a mean radius of curvature $\sim$0.5 mm). Here, we determine the potential distributions when the radius of a hemispherical droplet is moderately large compared to the Debye lengths, $\delta \gg 1$. In this analysis it is assumed that λ_d and λ_s are of similar magnitude; then ζ is of order unity.

Asymptotic expansions are straightforward to perform for the integrals and functions contained in equations (20) and (21). The asymptotic expansions take the form

$$\mathbf{f}_m \approx \mathbf{f}_m^{(2)} + \mathrm{o}(\delta^{-3}) \qquad \text{and} \qquad \mathbf{g}_m \approx \mathbf{g}_m^{(0)} + \mathbf{g}_m^{(2)} + \mathrm{o}(\delta^{-3}). \tag{25}$$

In these expressions, a superscript (j) on $\mathbf{f}_m$ or $\mathbf{g}_m$ indicates the asymptotic correction to order δ^{-j}; the exact forms of the correction terms are cumbersome, and are shown in appendix C.

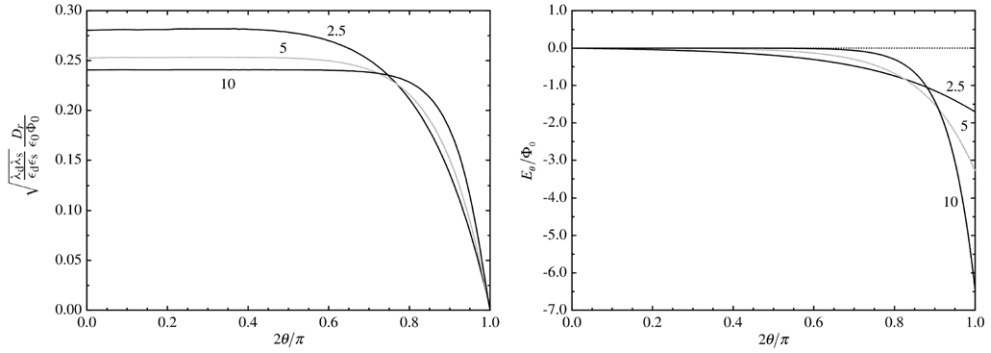

Figure 6. Field components along the liquid–liquid interface. Dimensionless normal electric displacement, $\sqrt{\frac{\lambda_d \lambda_s}{\epsilon_d \epsilon_s}} \frac{D_r}{\epsilon_0 \Phi_0}$, and tangential field, E_θ / Φ_0, as a function of polar angle for $\delta = 2.5$, 5, and 10.

One can see that the effect of the impermeable boundary dominates the potential distribution, because $\mathbf{g}_m = \mathrm{o}(\delta^0)$ and $\mathbf{f}_m = \mathrm{o}(\delta^{-2})$. Neither of the vectors has a correction of $\mathrm{o}(\delta^{-1})$. The matrix $\mathbf{C}_m$ can be expressed as

$$\mathbf{C}_m \approx \mathbf{C}_m^{(0)} + \mathbf{C}_m^{(1)} + \mathbf{C}_m^{(2)} + \mathrm{o}(\delta^{-3}), \tag{26}$$

and h_m takes the form

$$h_m \approx (\delta\zeta)^2 \left[h_m^{(0)} + h_m^{(1)} + h_m^{(2)} + \mathrm{o}(\delta^{-3}) \right]. \tag{27}$$

Again, the exact expressions for all four expansions are given in appendix C, equations (C.9)–(C.14).

Equations (25)–(27) allow determination of the Fourier–Legendre coefficients when a droplet is moderately large in comparison to the two Debye lengths. An asymptotic expansion of the potential distribution valid to order δ^{-1} can be determined from equation (22) by writing the Fourier–Legendre coefficients as

$$\begin{aligned} d_m &\approx d_m^{(0)} + d_m^{(1)} + \mathrm{o}(\delta^{-2}), \\ s_m &\approx s_m^{(0)} + s_m^{(1)} + \mathrm{o}(\delta^{-2}). \end{aligned} \tag{28}$$

The terms of highest order in δ are given by

$$\begin{bmatrix} d_m^{(0)} \\ s_m^{(0)} \end{bmatrix} = \phi^* \, (4m+3) \left(\mathbf{C}_m^{(0)} \right)^{-1} \mathbf{g}_m^{(0)}, \tag{29}$$

and those of the next lower order are

$$\begin{bmatrix} d_m^{(1)} \\ s_m^{(1)} \end{bmatrix} = - \left(\mathbf{C}_m^{(0)} + \mathbf{C}_m^{(1)} \right)^{-1} \mathbf{C}_m^{(1)} \begin{bmatrix} d_m^{(0)} \\ s_m^{(0)} \end{bmatrix}. \tag{30}$$

Note that the quantity $(\mathbf{C}_m^{(0)} + \mathbf{C}_m^{(1)})$ must be retained in this equation because $\mathbf{C}_m^{(1)}$ increases with m at constant δ, and hence is not always small compared to $\mathbf{C}_m^{(0)}$. To obtain ϕ^* to order δ^{-1}, one can use the charge-conservation relation, which expands to

$$\frac{1}{\phi^*} = \left[1 - 2 \sum_{m=0}^{\infty} \frac{d_m^{(0)} h_m^{(0)}}{\phi^*} \right] - 2 \sum_{m=0}^{\infty} \frac{d_m^{(0)} h_m^{(1)} + d_m^{(1)} h_m^{(0)}}{\phi^*} + \mathrm{o}(\delta^{-2}). \tag{31}$$

Each term with a summation is independent of ϕ^* because $d_m^{(0)}$ and $d_m^{(1)}$ are directly proportional to ϕ^*, as shown by equations (29) and (30). The bracketed term is $\mathrm{o}(\delta^0)$.

3.6. Very large droplets

In the limit when $\delta \to \infty$, the expansions are simplified dramatically. The zero-order terms in equations (27), (29), and (31) can be used to determine ϕ^*, which, after summing the infinite series over m, is given by

$$\lim_{\delta\to\infty} \phi^* = \frac{\chi^2 + \zeta^2}{3\chi^2 + \zeta^2}. \tag{32}$$

Substituting this relation into equation (29) shows

$$\begin{aligned} \lim_{\delta\to\infty} d_m &= \frac{(-1)^{m+1}\,\chi^2\,(4m+3)\,\Gamma(m+\frac{1}{2})}{2\sqrt{\pi}\left(3\chi^2+\zeta^2\right)\Gamma(m+2)}, \\ \lim_{\delta\to\infty} s_m &= \frac{(-1)^{m}\,\zeta^2\,(4m+3)\,\Gamma(m+\frac{1}{2})}{2\sqrt{\pi}\left(3\chi^2+\zeta^2\right)\Gamma(m+2)}. \end{aligned} \tag{33}$$

These two expressions can be inserted into equation (18) to demonstrate that the potential at the apex of the droplet is

$$\lim_{\delta\to\infty} \phi_{\text{apex}} = \frac{\zeta^2}{3\chi^2 + \zeta^2}. \tag{34}$$

Recall that in the case of large droplets, almost all of the interface retains the constant potential $\phi = \phi_{\text{apex}}$. It is interesting to find the angle along the droplet surface at which charge density is zero,

$$\sum_{m=0}^{\infty} \frac{(-1)^{m+1}\,(4m+3)\,\Gamma(m+\frac{1}{2})P_{2m+1}\,(\lim_{\delta\to\infty} x_{\text{zc}})}{\Gamma(m+2)} = 0, \tag{35}$$

which comes from equation (31). This equation shows that $\lim_{\delta\to\infty} x_{\text{zc}} = 0$; the line of three-phase contact has zero charge in phase d for very large droplets. The equation is independent of χ and ζ, revealing that this result in the infinite limit is the same for all combinations of electrolytic solutions in phases d and s when $\zeta = \text{o}(1)$ and $\delta \to \infty$.

3.7. Results for various droplet sizes

The values of ϕ^* and ϕ_{apex} yielded by the exact series, the first-order expansion, and the limiting expression valid when $\delta \to \infty$ are presented in figures 7 and 8. Both figures employ the parameters listed in table 1. With those parameters, $\lim_{\delta\to\infty} \phi^* = 0.4545$ and $\lim_{\delta\to\infty} \phi_{\text{apex}} = 0.1818$. Due to extremely slow convergence of the Fourier–Legendre series in the asymptotic expansion, five-digit numerical accuracy requires 27 000 terms; four significant figures can be achieved with 2000 terms.

Figure 7 shows that the first-order expansion predicts ϕ^* with great accuracy when $\delta \geqslant 10$, and that the $\delta \to \infty$ expression is very accurate when $\delta \geqslant 1000$. One should bear in mind when using the expansions for other cases that the relevant quantity is $\delta\zeta$ $(=r_{\text{d}}/\lambda_{\text{d}})$ rather than δ; for systems with different parameters, then, the exact solution is valid when $\delta\zeta \leqslant 12.25$, the first-order expansion agrees to the fifth significant figure when $12.25 < \delta\zeta \leqslant 1225$, and the infinite limit agrees to the fifth significant digit when $\delta\zeta > 1225$. Because most droplets investigated experimentally are of macroscopic dimensions ($\delta\zeta > 10^5$), this result shows that the expansion valid in the limit $\delta \to \infty$ is reasonable to use under most practical circumstances.

The potential at the droplet apex, ϕ_{apex}, is shown as a function of δ in figure 8. To generate this figure, the first-order asymptotic expansion was used when $\delta > 10$. When $\delta < 4.5$, ϕ_{apex} decreases as δ rises. Figures 3 and 4 provide a means by which to interpret this behaviour. They show that when δ is equal to 10, the charge is near zero across most of the droplet interior

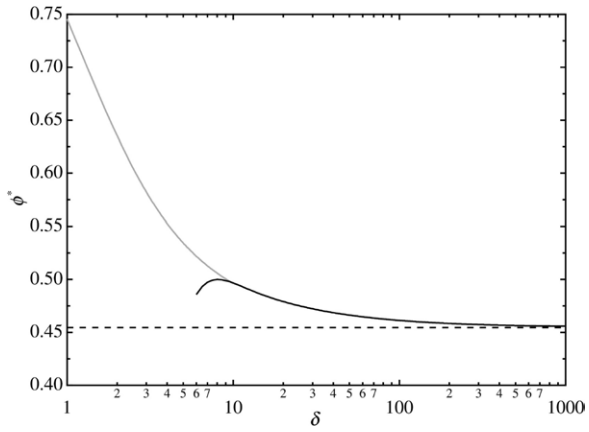

Figure 7. Exact and approximate solutions: semilog plot of ϕ^* as a function of δ. The exact solution is shown in grey, the first-order expansion is given by the black line, and the dashed line shows the limiting expression valid when $\delta \to \infty$.

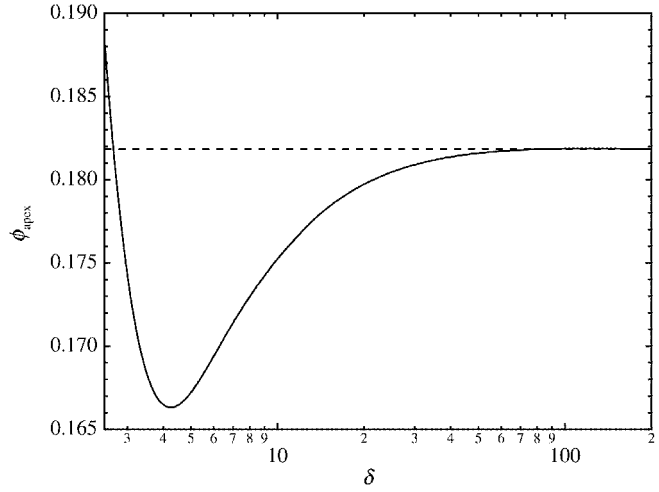

Figure 8. Nonmonotonic variation of the apex potential with droplet radius. Semilog plot of ϕ_{apex} as a function of δ. The black curve is a composite of the exact solution, used when $\delta \leqslant 10$, and the first-order expansion. The dashed line shows the limiting expression valid when $\delta \to \infty$.

and there is a plateau in potential near ϕ^*. The plateau does not exist when δ is 2.5 because the droplet radius is near the screening length. Charges near the electrode are not completely screened within the droplet; unscreened charge thus leads ϕ_{apex} to rise as δ decreases from 4.5.

At $\delta \approx 4.5$, the droplet is large enough to admit a potential plateau but remains sufficiently small compared to the screening length that the countercharges balancing the electrode-surface charge are impacted near the apex. This limits the amount of charge that can be accumulated at the surfaces, leading to a minimum in ϕ_{apex}. As δ increases from 4.5 the peak potential rises because balancing countercharges can distribute uniformly over a larger portion of the liquid–liquid surface—a trend also supported by figures 5 and 6. When δ grows very large, ϕ_{apex} tapers to a constant value; the range of electrode-charge screening decreases relative to the radius of

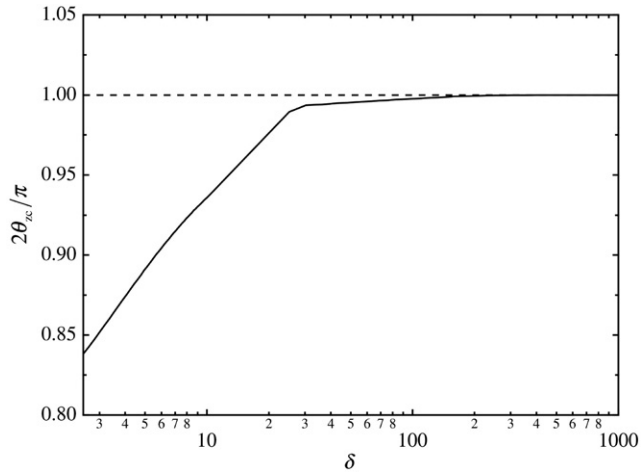

Figure 9. The angle of zero charge goes to the three-phase contact line with increasing radius. Semilog plot of θ_{zc} as a function of δ. The black curve is a composite of the exact solution, used when $\delta \leqslant 10$, and the first-order expansion. The dashed line shows the limiting expression valid when $\delta \to \infty$.

the droplet as δ rises, while the areas of the liquid–liquid interface and of droplet–electrode contact (through which electric fields pass) remain in fixed proportion.

Define the *angle of zero charge*, θ_{zc}, as the angle at which $P_e^d = 0$ on the inner droplet surface ($\theta_{zc} = \operatorname{acos} x_{zc}$). Note that $\lim_{\delta\to\infty} 2\theta_{zc}/\pi = 1$. Figure 9 shows this quantity as a function of δ.[4] The figure emphasizes the argument of the preceding paragraphs. When the droplet is small, the unscreened electrode charge covers a significant portion of the liquid–liquid interface. The angle of zero charge rapidly approaches $\pi/2$ when $\delta > 20$—the regime in which countercharges spread to cover most of the liquid–liquid interface uniformly. At $\delta = 1000$, the value of θ_{zc} differs from $\pi/2$ by less than 10^{-7}, suggesting that the surface charge reaches a constant value along the liquid–liquid interface over a distance less than a Debye length.

4. Truncated-spherical droplets

In reality, the contact angle of the oil–water interface is determined by the degree of polarization and the three surface tensions between oil, water, and substrate. It has been observed experimentally that, for nitrobenzene droplets surrounded by water on a glassy carbon substrate at zero polarization, the contact angle is 95° [27]. In these experiments the contact angles were found to increase with increased applied potential. A droplet of initial radius 1 mm ($V_d \approx 20\ \mu$l) was shown to retain a truncated-spherical shape up to a polarization of 1 V. It is reasonable to expect that the electrolytic system behaves similarly. In fact, a subsequent

[4] The droplet-apex potential and ϕ^* can be determined solely from the Fourier–Legendre coefficients without any evaluations of special functions in the potential distributions (equations (18)). However, the computation of θ_{zc} requires numerically accurate Legendre polynomials at large m. High-precision Legendre polynomials were obtained to generate figure 9 by the trigonometric series

$$P_{2m+1}(\cos\theta) = \frac{\binom{4m+2}{2m+1}}{2^{4m+1}} \sum_{k=0}^{m} \left[\binom{2m+1}{k^2} \Big/ \binom{4m+2}{2k} \right] \cos\left[(2m-2k+1)\,\theta\right],$$

which can be derived by induction with one of the expansion methods from [26]. The terms in the summation decrease absolutely with increasing k when $\theta = 0$.

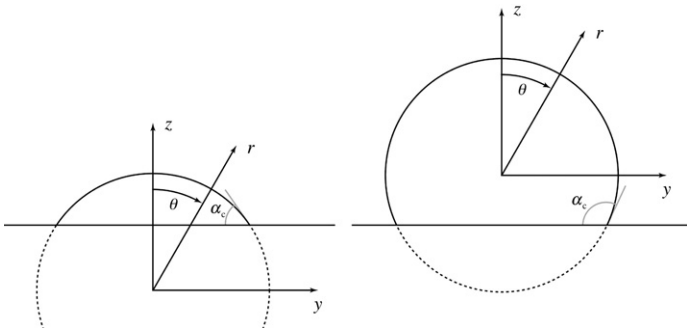

Figure 10. Sketch of truncated-spherical droplets, for acute contact angles (left) and obtuse contact angles (right).

section provides a theoretical justification for the assertion that a truncated sphere is the most energetically favorable droplet shape. As a preliminary step towards that analysis, we first examine the electrostatics when droplets take fixed truncated-spherical shapes.

4.1. Parameterization of shape

Truncated-spherical droplet shapes are shown in figure 10. In this analysis, the contact angle with the electrode, α_c, is assumed to be known. It may be acute or obtuse, as shown in the figure. The figure places the origin of coordinates at the geometric centre of the sphere, which leaves the governing equations identical to equations (12) and keeps the potential- and electric displacement-matching equations at a fixed value of ξ. In addition, the definitions of x, ξ, ϕ_d, ϕ_s, ϕ^*, ζ, χ, and δ remain the same. For truncated-spherical droplets, δ is independent of θ.

Although the governing equations are most easily solved in terms of the radius of curvature, droplet volume is the fixed experimental parameter. It is therefore useful to relate the radius of curvature to the droplet volume through

$$\delta = \frac{1}{\sqrt{\lambda_d \lambda_s}} \left[\frac{3V_d}{\pi \left(2 - 3\cos\alpha_c + \cos^3\alpha_c\right)} \right]^{\frac{1}{3}}. \tag{36}$$

This equation also depends on the contact angle α_c. In the following analysis, V_d is taken as fixed to regularize the droplet size; δ then varies with α_c only.

In further discussion, it will also be necessary to consider the liquid–liquid and electrode–droplet interfacial areas. Let S_A^{ds} denote the surface area of the liquid–liquid interface, and S_A^{de} denote the area of droplet–electrode contact. A significant parameter that arises is the ratio of these areas, $\eta = S_A^{ds}/S_A^{de}$. For truncated-spherical droplets,

$$\eta = \frac{1}{\cos^2(\frac{1}{2}\alpha_c)} \tag{37}$$

expresses the ratio of areas in terms of the contact angle. This definition differs when droplets take alternative shapes.

4.2. The large-droplet approximation

As the analysis of hemispherical droplets has shown, when $\delta\zeta \gg 10^3$ the droplet can be considered as 'infinitely large'. Only this regime will be treated because it applies in almost all experiments. Also, it was demonstrated for hemispheres that when $\delta\zeta \gg 10^3$ a vast majority

of the liquid–liquid interface maintains a constant potential and null tangential field. The potential does change along the liquid–liquid interface in a very small region near the line of three-phase contact; this region can be neglected because it makes a negligible contribution to the total electrostatic energy. (The discussion in appendix D rigorously justifies this aspect of the approximation.) Because the polar-angle dependence of potential is negligible over the vast majority of the liquid–liquid interface, its curvature can be neglected. The liquid–liquid interface and the droplet–electrode interface may be treated as separate one-dimensional regions, with surface charges related through the constant bulk potential ϕ^*. The adoption of these assumptions for droplets with $\delta\zeta \gg 10^3$ is referred to here as the 'large-droplet approximation'.

4.3. Potentials in the large-droplet approximation

We first adopt the large-droplet approximation to examine the potential distribution near the liquid–liquid interface. This region is considered semi-infinite in both directions normal to the interface, and its curvature is neglected. Let z' denote a coordinate along the outward normal of the droplet surface, with $z' = 0$ at the interface. Potential distributions that satisfy potential- and electric displacement-matching conditions at $z' = 0$ are

$$\begin{aligned} \phi_{\mathrm{d}}^{\mathrm{ds}} &= \phi^* - \frac{\phi^* \chi^2}{\chi^2 + \zeta^2} \mathrm{e}^{\frac{\zeta z'}{\sqrt{\lambda_{\mathrm{d}}\lambda_{\mathrm{s}}}}}, \qquad z' \leqslant 0, \\ \phi_{\mathrm{s}}^{\mathrm{ds}} &= \frac{\phi^* \zeta^2}{\chi^2 + \zeta^2} \mathrm{e}^{-\frac{z'}{\zeta\sqrt{\lambda_{\mathrm{d}}\lambda_{\mathrm{s}}}}}, \qquad z' \geqslant 0, \end{aligned} \tag{38}$$

where a superscript ds denotes the potential near the liquid–liquid interface. These distributions are similar to ones obtained in the linear approximation for a planar ITIES (with no compact solvent layer between solutions) [28].

Under the large-droplet approximation, the droplet–electrode interface may also be treated as a semi-infinite planar region. Let a superscript de denote contributions to the potential arising from the droplet–electrode interface, and se denote those from the surrounding solution–electrode interface. Taking linearized PB equations with $\phi_{\mathrm{d}}^{\mathrm{de}} = \phi_{\mathrm{s}}^{\mathrm{se}} = 1$ at the electrode surface, $\lim_{z\to\infty} \phi_{\mathrm{d}}^{\mathrm{de}} = \phi^*$, and $\lim_{z\to\infty} \phi_{\mathrm{s}}^{\mathrm{se}} = 0$, one obtains

$$\phi_{\mathrm{d}}^{\mathrm{de}} = \left(1 - \phi^*\right) \mathrm{e}^{-\frac{\zeta z}{\sqrt{\lambda_{\mathrm{d}}\lambda_{\mathrm{s}}}}} + \phi^* \qquad \text{and} \qquad \phi_{\mathrm{s}}^{\mathrm{se}} = \mathrm{e}^{-\frac{z}{\zeta\sqrt{\lambda_{\mathrm{d}}\lambda_{\mathrm{s}}}}}, \tag{39}$$

familiar forms from the planar double-layer theory.

To retrieve the value of ϕ^*, the charges contained in regions ds and de within the droplet are set to be equal and opposite. This is most easily performed by using surface integrals of the fields around the droplet boundary. At this stage, we adopt the second part of the large-droplet approximation and neglect the small region near the line of three-phase contact where the potential changes along surface ds. A charge balance by surface integrals of the fields shows that

$$\phi^* = \frac{\chi^2 + \zeta^2}{\chi^2 (1 + \eta) + \zeta^2} \tag{40}$$

gives ϕ^* (recall that equation (37) defines η for truncated spheres). The potential at the liquid–liquid interface, $\phi_j^{\mathrm{ds}}(\delta)$, is then

$$\phi_j^{\mathrm{ds}}(\delta) = \frac{\zeta^2}{\chi^2 (1 + \eta) + \zeta^2}. \tag{41}$$

When the contact angle is $\pi/2$, $\eta = 2$, and these equations agree with the analogous results derived for large hemispheres, equations (32) and (34).

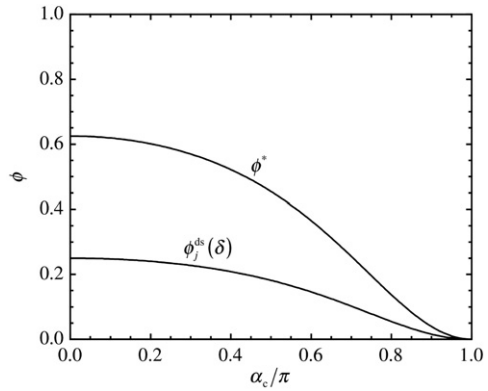

Figure 11. The droplet bulk potential and liquid–liquid interface potential decrease monotonically with respect to contact angle. Plot of ϕ^* and $\phi_j^{ds}(\delta)$ as a function of contact angle for a 0.01 M nitrobenzene droplet surrounded by a 0.01 M aqueous solution.

Figure 11 shows the values of ϕ^* and $\phi_j^{ds}(\delta)$ as a function of contact angle for a system with the parameters given in table 1. The figure shows that in the limit of nonwetting both potentials go to zero: the interior of the droplet maintains no concentration gradients when α_c goes to π. Both potentials also fall monotonically with the contact angle; their maximum values in the limit of complete wetting are determined by the values of ζ and χ. The maximum charge density that the surrounding solution can maintain near the droplet surface is proportional to $-\phi_j^{ds}(\delta)$; thus, as the droplet contracts, the density of countercharges in the surroundings decreases. This tendency is the same at all values of χ and ζ.

4.4. Electrostatic energy in the large-droplet approximation

The electrostatic contribution to the free energy during polarization of phase i in region j, $\mathscr{E}_i^j$, is

$$\mathscr{E}_i^j = -\frac{\epsilon_0}{2}\int_{V_i^j} \epsilon_i \mathbf{E}_i \cdot \mathbf{E}_i \, \mathrm{d}V + \frac{1}{2}\int_{V_i^j} \rho_e^i(\Phi_i - \Phi_i^{ref}) \, \mathrm{d}V, \tag{42}$$

where $\mathbf{E}_i = -\nabla\Phi_i$ is the electric field and V_i^j is the volume of phase i in region j; Φ_i^{ref} denotes the reference potential appropriate to phase i ($\Phi_d^{ref} = \Phi^*$ and $\Phi_s^{ref} = 0$). As a reference state for the energy, we choose the planar-electrode system in the absence of the droplet—that is, a system with identical electrode geometry, but with only the surrounding solution separating the electrodes. The polarization energy of this reference state is denoted $\mathscr{E}_0$. It is obtained by insertion of the solution for planar Debye screening into equation (42) and integration over the entire system volume. This choice of reference state eliminates the need to know the contact area of the surrounding solution and the electrode.

Under the large-droplet approximation, the polarization energy relative to that of the reference state, $\Delta\mathscr{E}$, defined as

$$\Delta\mathscr{E} = \mathscr{E}_d^{ds} + \mathscr{E}_s^{ds} + \mathscr{E}_d^{de} + \mathscr{E}_s^{se} - \mathscr{E}_0, \tag{43}$$

is given by the equation

$$\lim_{\delta\to\infty} \frac{\Delta\mathscr{E}}{2\pi\epsilon_0\Phi_0^2\sqrt{\lambda_d\lambda_s\epsilon_d\epsilon_s}} = \chi\left[\frac{1}{\zeta} - \frac{\zeta\eta}{\chi^2(1+\eta)+\zeta^2}\right]\frac{\delta^2(\eta-1)}{\eta^2}. \tag{44}$$

To derive this equation, regions ds and de were treated as semi-infinite in the volume integrals, in accord with the large-droplet approximation. Appendix D justifies the neglect of energetic contributions from the region near the three-phase contact line.

5. Potential dependence of droplet shape

The previous sections have provided an understanding of the electrostatics of polarized electrolytic droplets in immiscible electrolytic solutions with fixed droplet shape. Here, we relax this condition and include the surface-tension forces that also affect the shape. It is assumed here that the large-droplet approximation applies even when droplets are not truncated spheres, provided that $V_\mathrm{d} > 2\pi(1225\lambda_\mathrm{d})^3/3$. Because the electrostatics have been evaluated explicitly, the surface tensions may be assumed independent of potential.

5.1. Droplet shape by free-energy minimization

When the droplet shape is not fixed, the electrostatic potentials are still given by equations (38) and (39); also, η retains its original definition as the ratio of surface areas, $\eta = S_A^\mathrm{ds}/S_A^\mathrm{de}$. However, equations (36) and (37), which are specific to truncated spheres, no longer hold. The electrostatic energy relative to that of a reference state with no droplet is given by

$$\Delta\mathscr{E} = \frac{\epsilon_0\Phi_0^2}{2}\sqrt{\frac{\epsilon_\mathrm{d}\epsilon_\mathrm{s}}{\lambda_\mathrm{d}\lambda_\mathrm{s}}}\left[\frac{\chi^2-\zeta^2\,(1-\phi^*)^2}{\chi\zeta}S_A^\mathrm{de} - \frac{\chi\zeta\,(\phi^*)^2}{\zeta^2+\chi^2}S_A^\mathrm{ds}\right]. \tag{45}$$

Note that the value of ϕ^* depends on η through equation (40), the derivation of which did not require the droplet to be a truncated sphere.

Also, the energy arising from surface-tension forces relative to the droplet-free reference state, $\Delta\mathscr{C}$,

$$\Delta\mathscr{C} = \gamma_\mathrm{ds}S_A^\mathrm{ds} + (\gamma_\mathrm{de}-\gamma_\mathrm{se})\,S_A^\mathrm{de}, \tag{46}$$

contributes to the free energy. In the capillary energy $\Delta\mathscr{C}$, γ_{ij} is the surface tension between phase i and j. A subscript e denotes the electrode.

The system free energy relative to the reference state with no droplet, ΔG, is

$$\Delta G = \Delta\mathscr{C} + \Delta\mathscr{E}. \tag{47}$$

An optimal droplet shape is one that minimizes ΔG.

Eventually, it follows from equations (45)–(47) that the optimal shape of the droplet is a truncated sphere. Inserting equations (45) and (46) into equation (47) gives the free energy more explicitly as

$$\begin{aligned}\Delta G = &\left[\gamma_\mathrm{ds} - \frac{\epsilon_0\Phi_0^2\chi\zeta\,(\phi^*)^2}{2\left(\zeta^2+\chi^2\right)}\sqrt{\frac{\epsilon_\mathrm{d}\epsilon_\mathrm{s}}{\lambda_\mathrm{d}\lambda_\mathrm{s}}}\right]S_A^\mathrm{ds}\\ &+\left[\gamma_\mathrm{de}-\gamma_\mathrm{se}+\frac{\epsilon_0\Phi_0^2\left[\chi^2-\zeta^2\,(1-\phi^*)^2\right]}{2\chi\zeta}\sqrt{\frac{\epsilon_\mathrm{d}\epsilon_\mathrm{s}}{\lambda_\mathrm{d}\lambda_\mathrm{s}}}\right]S_A^\mathrm{de}.\end{aligned} \tag{48}$$

The first bracketed term on the right will be denoted γ_ds^* in the subsequent discussion to simplify notation.

To determine the droplet shape, one must perform the minimization of ΔG with V_d fixed. We designate this constraint on the droplet volume by V. An additional constraint must be included to express the conservation of ion numbers in the droplet. Equation (40) expresses

this conservation under the large-droplet approximation. By replacing η in equation (40) with the ratio of surface areas, one obtains a constraint on the net droplet charge, Q, defined as

$$Q = \Phi_0 \left[\left(1 - \phi^*\right) \left(\chi^2 + \zeta^2\right) S_A^{\mathrm{de}} - \phi^* \chi^2 S_A^{\mathrm{ds}} \right] = 0. \tag{49}$$

This determines ϕ^* such that the net charge in the droplet is zero. The value of Φ_0 is included in this definition so that Q is trivially zero when there is no applied potential.

Let v denote a coordinate extending from the droplet apex (at $v = 0$) through an outward normal of the electrode surface, and let $W(v)$ give a member of the family of curves that describe the radius of the droplet perpendicular to this axis ($W(0) = 0$). Both surface areas contained in ΔG, V, and Q are functionals of $W(v)$: $S_A^{\mathrm{ds}}[W]$ and $S_A^{\mathrm{de}}[W]$. The droplet shape is determined by minimizing $\Delta G[W] - \lambda V[W] - \mu Q[W]$ with respect to $W(v)$, where λ and μ are Lagrange multipliers.

The surface area of the liquid–liquid interface depends on $W(v)$ through

$$S_A^{\mathrm{ds}}[W] = 2\pi \int_0^{v_0} W \sqrt{1 + (W')^2}\, \mathrm{d}v, \tag{50}$$

where v_0 denotes the position of the electrode relative to the droplet apex. The area of the region of droplet–electrode contact is

$$S_A^{\mathrm{de}}[W] = \pi W^2(v_0). \tag{51}$$

A suitable definition for the volume-constraining functional $V[W]$ is

$$V[W] = \pi \int_0^{v_0} W^2\, \mathrm{d}v, \tag{52}$$

because the droplet is symmetric about the axis through its apex.

Taking the variation of the free-energy functional with respect to W and setting it to zero, one obtains the augmented Young–Laplace equation

$$\frac{1}{W[1 + (W')^2]^{\frac{1}{2}}} - \frac{W''}{[1 + (W')^2]^{\frac{3}{2}}} = \frac{\lambda}{\gamma_{\mathrm{ds}}^* + \mu \Phi_0 \phi^*}. \tag{53}$$

When taking the variation, a boundary condition on this equation at v_0 also arises because the endpoint of W is not fixed. It has a complicated algebraic form, and is omitted here.

Equation (53) is satisfied if $W(v)$ describes a circular arc with radius of curvature $r_{\mathrm{d}} = 2(\gamma_{\mathrm{ds}}^* + \mu \Phi_0 \phi^*)/\lambda$ and infinite slope at $W(0) = 0$. The multipliers μ and λ can be determined in terms of v_0 through equations (49) and (52); the boundary condition at v_0 then specifies the other endpoint of the arc in terms of the original parameters. Therefore, the circular-arc trial function provides a unique solution to the governing equations. This concludes the proof that truncated-spherical shapes are optimal when droplets are polarized.

5.2. Reparameterization of shape

Obtaining v_0 through the boundary condition that arises on the Young–Laplace equation is possible, but very algebraically intensive. It is simpler at this stage to exploit the fact that equation (53) is satisfied by truncated spheres and return to the functional for free energy. Then, all of the geometric variables in equation (47) can be parameterized in terms of the contact angle, which is related to η in equation (37). This provides a simple function for ΔG, which can be minimized with respect to contact angle to find the optimal free energy.

The quantity η should be replaced with a more directly accessible experimental parameter. It is more intuitive to think in terms of contact angles; η can be replaced by the cosine of the

contact angle, x_c, as the independent variable in ΔG. With equation (37), it can be shown by trigonometric identity that η is related to x_c through

$$x_c = \frac{2-\eta}{\eta}. \tag{54}$$

This variable has the added advantage that when surface-tension forces are included, its value at zero polarization, x_c^0, is given by the Young equation,

$$x_c^0 = \frac{\gamma_{se} - \gamma_{de}}{\gamma_{ds}}. \tag{55}$$

Equation (36) and the definition of x_c allow the surface areas of the interfaces ds and de to be stated in terms of the contact-angle cosine and droplet volume,

$$S_A^{ds} = 2V_d^{\frac{2}{3}}\left[\frac{9\pi}{(1-x_c)(2+x_c)^2}\right]^{\frac{1}{3}} \quad \text{and} \quad S_A^{de} = V_d^{\frac{2}{3}}\left[\frac{9\pi\,(1+x_c)^3}{(1-x_c)(2+x_c)^2}\right]^{\frac{1}{3}}. \tag{56}$$

Substitution of these relations and equations (40) and (54) into equation (45) provides an expression for $\Delta\mathscr{E}$,

$$\Delta\mathscr{E} = \frac{\epsilon_0\Phi_0^2 V_d^{\frac{2}{3}}}{2}\sqrt{\frac{\epsilon_d\epsilon_s}{\lambda_d\lambda_s}}\chi\left[\frac{9\pi\,(1+x_c)^3}{(1-x_c)(2+x_c)^2}\right]^{\frac{1}{3}}\left[\frac{1}{\zeta} - \frac{2\zeta}{\chi^2(3+x_c)+\zeta^2(1+x_c)}\right]. \tag{57}$$

An expression can also be retrieved for the capillary energy term, $\Delta\mathscr{C}$, by insertion of equations (55) and (56) into (46),

$$\Delta\mathscr{C} = \gamma_{ds}V_d^{\frac{2}{3}}\left[\frac{9\pi}{(1-x_c)(2+x_c)^2}\right]^{\frac{1}{3}}[2 - x_c^0(1+x_c)]. \tag{58}$$

This completes the reparameterization in terms of the contact-angle cosine, x_c.

5.3. Contact angle by free-energy minimization

Equations (57) and (58) can be inserted into equation (47), reducing ΔG to a simple function of Φ_0, V_d, and x_c. The contact-angle cosine is then determined by minimizing this function with respect to x_c at fixed Φ_0 and V_d. In fact, because S_A^{ds} and S_A^{de} are both proportional to $V_d^{2/3}$, the equation that gives the contact angle is independent of the droplet volume, leaving Φ_0 as the only free parameter if the composition of the system is specified.

Minimization of the free-energy function with respect to the contact-angle cosine yields the formula

$$x_c - x_c^0 = \frac{\epsilon_0\Phi_0^2}{2\gamma_{ds}}\sqrt{\frac{\epsilon_d\epsilon_s}{\lambda_d\lambda_s}}\chi\zeta\left[\frac{\left(\chi^2+\zeta^2\right)x_c\,(1+x_c)^2 + 4\chi^2}{\left[\chi^2(3+x_c)+\zeta^2(1+x_c)\right]^2} - \frac{1}{\zeta^2}\right]. \tag{59}$$

Under polarization, this transcendental equation determines the cosine of the contact angle as a function of potential. With no applied potential this expression reduces to the standard Young equation, $x_c - x_c^0 = 0$.

5.4. Results for nitrobenzene/water

The surface tension between nitrobenzene and water is $\gamma_{ds} = 25.5$ mJ m^{-2} [31]; the contact angle of an unpolarized nitrobenzene droplet surrounded by water on a glassy carbon substrate is 95° [27], which shows that $x_c^0 = (\gamma_{se} - \gamma_{de})/\gamma_{ds} = -0.0872$. These parameters and those in table 1 allow calculation of the contact angle as a function of potential by equation (59). The result is shown in figure 12, which demonstrates that the contact angle increases with

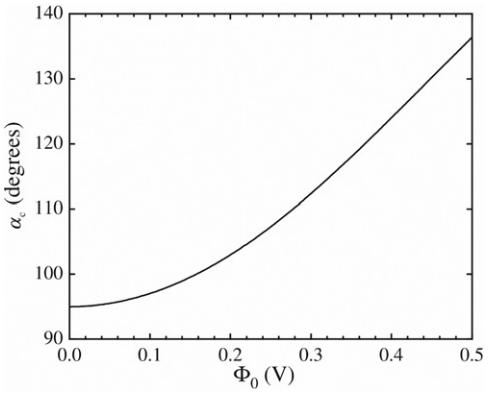

Figure 12. Contraction of a droplet with potential. Contact angle, $\alpha_c = \text{acos}\, x_c$, as a function of applied potential for a 0.01 M nitrobenzene droplet surrounded by a 0.01 M aqueous solution.

potential. When polarized, the droplet tends to contract. Because Φ_0^2 appears in equation (59), this happens whether the applied potential is positive or negative.

The tendency of a nitrobenzene droplet to contract agrees with expectations: contraction has been observed in the electrolyte-free nitrobenzene/water system [27]. This might be expected on the basis that water is more polar than nitrobenzene, and hence tends to cover more of the electrode when the metal is held at fixed potential. We specially considered an opposite situation, in which the solutions composing the droplet and the surroundings were exchanged—the case $\chi = 0.67$, $\zeta = 0.8$, $x_c^0 = 0.0872$. In this case, the droplet was also found to contract with increasing polarization (although less strongly). This is somewhat surprising. From the perspective of solvent polarity, one might expect an expansion if the dielectric constant of the droplet was higher than that of its surroundings.

To understand why the droplet still contracts when the solutions in the two phases are switched, one must consider that a balance of surface-tension forces and electrostatic forces determines the contact angle. Surface forces always tend to draw the system back to the contact angle at null polarization, which minimizes the surface energy. By contrast, electrostatic forces drive the system toward a contact angle that maximizes the total capacitance, minimizing the electrostatic energy. The droplet contracts when the contact angle that maximizes capacitance is larger than the zero-polarization contact angle, and expands when the capacitance-maximizing contact angle is smaller.

Our primary focus has been an organic droplet/aqueous surroundings system in which the specific capacitance of the droplet–electrode interface is lower than that of the interface between the surroundings and the electrode ($\chi/\zeta > 1$). For systems of this type, the capacitance of a system without a droplet is higher than that of a system with a droplet on the electrode; electrostatic forces thus drive the system toward the limit of nonwetting (a contact angle of π). In such cases, the droplet shape at which surface and electrostatic forces balance always occurs at a contact angle larger than the zero-polarization angle. Hence, when $\chi/\zeta > 1$, the droplet contracts.

By contrast, from the perspective of electrostatics one might expect the optimal state to be complete wetting when the droplet–electrode interface has a higher specific capacitance than the interface between the outer solution and the electrode ($\chi/\zeta < 1$). However, the situation is not this simple because conservation of ionic masses within the droplet reduces the amount of charge that can accumulate at its inner interfaces. When the droplet–electrode interface

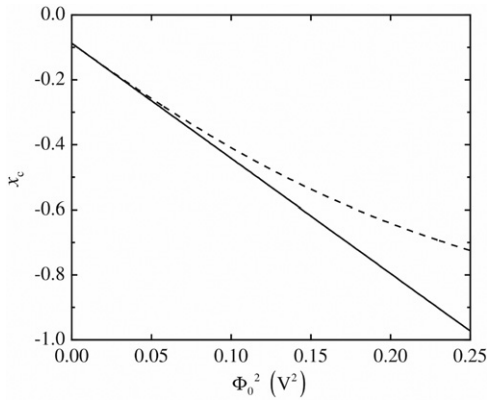

Figure 13. At small potentials, the contact-angle cosine is linear with potential squared. Comparison of x_c determined from the approximation in equation (61) (solid line) to the exact result from transcendental equation (59) (dashed line) for a 0.01 M nitrobenzene droplet surrounded by a 0.01 M aqueous solution.

expands, there is a balance between the added specific capacitance and the inhibition of charge accumulation due to overall droplet electroneutrality. Thus, if $\chi/\zeta < 1$, the electrostatically optimal contact angle lies somewhere in the regime of partial wetting. This optimizing angle may be greater than or less than the zero-polarization contact angle. Hence, the droplet can either contract or expand. In the case of a 0.01 M aqueous droplet surrounded by a 0.01 M solution in nitrobenzene, the electrostatically optimal contact angle remains greater than the zero-polarization contact angle: the droplet contracts.

5.5. Surface tension measurement by contact angle-potential plots

Although equation (59) provides a relatively straightforward means by which to compute the contact angle as a function of potential, it is still a transcendental equation. A simpler formula can be obtained by perturbation when the right-hand side of equation (59) is small. By defining the *response function*, $K(p,q)$,

$$K(p,q) \equiv p\left[\frac{q\,(1+q)^2\left(1+p^2\right)+4p^2}{\left[p^2\,(3+q)+(1+q)\right]^2}-1\right], \tag{60}$$

a first-order approximation to equation (59) can be written as

$$x_c - x_c^0 = \frac{\epsilon_0\Phi_0^2}{2\gamma_{ds}}\sqrt{\frac{\epsilon_d\epsilon_s}{\lambda_d\lambda_s}}K\left(\frac{\chi}{\zeta}, x_c^0\right). \tag{61}$$

Figure 13 compares contact-angle cosines obtained from the transcendental equation (59) to those given by the approximate formula, equation (61). It shows that the approximation matches the transcendental relation almost exactly at potentials less than 0.2 V ($\Phi_0^2 < 0.04\,\mathrm{V}^2$). This potential range is well beyond the upper limit of validity of the linearized PB equations. Thus, the approximate equation is reasonable to use at all potentials for which the linear theory is valid.

The dielectric properties and Debye lengths are typical parameters to set in an experiment (note that $\chi/\zeta = \sqrt{\epsilon_s\lambda_d/\epsilon_d\lambda_s}$). With these and a measurement of the cosine of the zero-polarization contact angle, x_c^0, equation (61) provides a way to obtain the liquid–liquid surface tension γ_{ds} from a linear fit of contact-angle cosines versus Φ_0^2.

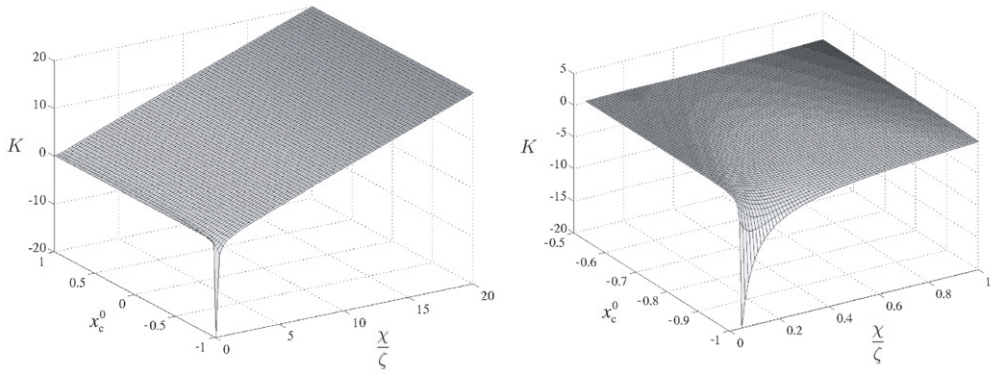

Figure 14. Variation of the response function with system parameters. Plot of $K(\chi/\zeta, x_c^0)$. When K is negative the droplet expands with polarization; when it is positive the droplet contracts. The magnitude of K determines the degree of expansion or contraction. The graph on the left shows K over a practical range of system parameters; the graph on the right shows in detail the range $\chi/\zeta < 1$; the droplet may expand in this range of solution properties when $x_c^0 < -0.64$.

One should also note from figure 13 that the exact solution to the transcendental equation deviates upward from the approximate form as potential increases. At small values of Φ_0, $x_c - x_c^0$ is proportional to Φ_0^2 with negative slope, and at large values of Φ_0, $x_c - x_c^0$ is proportional to Φ_0 with negative slope. Although the dependence of the contact-angle cosine on Φ_0 weakens, it does not reach a constant asymptote—this suggests that contact-angle saturation does not occur in the three-phase solid/ITIES system. However, this result is inconclusive: the linear PB analysis presented here is restricted to small potentials, and the linear approximation is only strictly valid in the region where x_c is proportional to Φ_0^2. The issue of contact-angle saturation will be addressed in future work on the nonlinear PB analysis.[5]

5.6. Shape response as a function of system parameters

It is worthwhile exploring how the parameters in equation (61) determine the response of the droplet to polarization. By insertion of the definition of Debye length (equation (5)) into the prefactor of K, one can see that the degree of expansion or contraction with potential can be enhanced by increasing the electrolyte concentrations while leaving their ratio fixed. One should bear in mind that x_c^0 can also be affected by the bulk salt concentrations in the two phases.

A more interesting quantity to explore is the response function K: its sign determines whether the droplet expands or contracts upon polarization, and its magnitude determines the degree of expansion or contraction. Figure 14 shows the variation of the response function with system properties. For combinations of the parameters where K is negative, the droplet expands with polarization; if K is positive, the droplet contracts. The figure shows that the contact-angle cosine must be less than -0.64 for expansion to occur. The liquid–liquid surface tension must therefore be relatively low, and the zero-polarization contact angle must be obtuse, for polarization to cause droplet expansion. This suggests that in cases where $x_c^0 < 0$, droplet

[5] A suggested cause for contact-angle saturation in pure-dielectric electrowetting systems is the increase of field divergence near the three-phase contact line with increasing contact angle [32]. Appendix D shows that the contribution of the three-phase contact region to the total electrostatic energy is negligible over all contact angles in the solid/ITIES system when the large-droplet approximation is valid. If field divergence near the three-phase contact line is the mechanism of contact-angle saturation, then saturation would not be expected in the systems treated here.

shapes may be stabilized with respect to potential by the addition of electrically neutral surface-tension lowering surfactants.

Figure 14 also furthers the previous qualitative discussion of the roles of surface-tension and electrostatic forces. As the surface tension at the liquid–liquid interface falls ($x_c^0 \to -1$), the range of χ/ζ over which the droplet expands increases. The plane $x_c^0 = -1$ in the figure, which corresponds to the lower limit of liquid–liquid surface tension, supports the argument that electrostatics drive the system toward the capacitance-maximizing shape. When the liquid–liquid surface forces are removed, contraction occurs when $\chi/\zeta > 1$ (the surroundings have higher specific capacitance), and expansion occurs when $\chi/\zeta < 1$.

6. Conclusion

The physics of droplet electrowetting with two immiscible electrolytic solutions differs greatly from that with two immiscible pure-dielectric liquids. In the electrolytic system, the polarized electrode surface draws droplet-phase ions toward the electrode, which causes an accumulation of counterions at the liquid–liquid interface: the droplet has an ion-impermeable boundary, and therefore must have zero total charge. At the polarized liquid–liquid interface, double layers form in both the droplet phase and the surrounding solution. This work provides the first theory to describe electrowetting with ITIES.

A minor modification of the Boltzmann distribution can describe the inhibition of ion motion by the droplet boundary. In hemispherical droplets, the distributions yielded by an exact solution of the resulting modified linearized PB equations show that the countercharges drawn to the liquid–liquid interface are localized in a region that extends only a few Debye lengths from the surface. This localized charging still occurs when the droplet's mean radius of curvature is very much larger than the Debye lengths. When a droplet is large, the entire liquid–liquid interface maintains a nearly constant potential, and hence, a nearly constant surface-charge density. Away from the interfaces, most of the interior of a large droplet resides at a constant potential that lies between the electrode and liquid–liquid surface potentials.

Capillary forces determine the shape of an unpolarized droplet. At zero polarization, the free-energy minimizing droplet shape is a truncated sphere, and this remains true when the system is polarized. If the volume of the droplet is fixed, as it would be in experiments, all governing relationships can be expressed easily in terms of a single geometric parameter: the contact angle between the liquid–liquid surface and the electrode.

When contact angles deviate from perpendicular, the electrostatic response is essentially similar to the hemispherical case. The field tangential to the liquid–liquid interface diverges near the three-phase contact line in hemispheres, and may diverge more strongly if the contact angle changes. However, the divergence at all contact angles is sufficiently weak that the contribution of this field singularity to the total electrostatic energy (and the change in total electrostatic energy with respect to contact angle) is small. Neglect of the three-phase contact region is rigorously valid when the droplet's mean radius of curvature is much greater than 10^3 droplet-phase Debye lengths. In that size regime, the polar-angle dependence of potential can be neglected.

Surface tension always tends to pull a droplet back to its unpolarized contact angle. Electrostatic forces tend to move the contact angle to one that maximizes the system capacitance. These two effects determine the polarization response. If the capacity-maximizing contact angle is smaller than the unpolarized contact angle, the droplet will expand upon polarization. Expansion happens when liquid–liquid surface tensions are relatively low, the zero-polarization contact angle is obtuse, and the inner area-specific capacitance is higher than the outer. Otherwise the droplet contracts.

Contraction or expansion of an electrolytic droplet surrounded by an immiscible electrolytic solution is determined by the solution compositions, the applied potential, the zero-polarization Young angle, and the liquid–liquid surface tension. At small potentials a simple law, equation (61), gives the contact angle as a function of these parameters. The formula can be used to obtain the magnitudes of liquid–liquid surface tensions from experimental contact angle/potential plots, and may be useful for experimentalists.

As a final note, it should be mentioned that the physics presented here may be practically applicable to phase-transfer catalysis [33, 34]. The potential in the bulk of the droplet, Φ^*, can play an important role in cases where charge-transfer processes occur at the liquid–liquid interface. When ions transferable across the interface are present, the bulk potential defines the ionic equilibrium (that is, the potential partition) between the droplet and the surrounding phase. Although this work does not apply to systems where Faradaic processes occur, it may be possible to extend the theory in this direction. It would be logical to approach first the cases in which dilute reactants are well supported by two immiscible electrolytic solutions.

Acknowledgments

This work was made possible by the generous support of the Leverhulme Trust Interchange Grant (F/07058/P). Our attention was drawn to this system by Hubert Girault during a workshop at Imperial College, 'ITIES: What Next?', supported by the same grant. The authors also thank Sasha Kuznetsov for consultations during his stay as a Leverhulme Visiting Professor at Imperial College. M Urbakh gratefully acknowledges the Israel Science Foundation (grant 773/05) for additional financial support. C Monroe would like to thank Suzanne Antink and Misha Vereyken, who laid the groundwork for equations (32) and (37).

Appendix A. Computation of integrals for arbitrarily sized hemispherical droplets

Analytical forms for the integrals contained in $\mathbf{f}_m$ are given by

$$\int_0^1 \mathrm{e}^{-ax} P_{2m+1}(x)\,\mathrm{d}x = \frac{{}_1F_2(\{1\},\{\frac{1}{2}-m,2+m\},\frac{a^2}{4})\sqrt{\pi}}{2\Gamma(\frac{1}{2}-m)\Gamma(2+m)} - \sqrt{\frac{\pi}{2a}} I_{2m+\frac{3}{2}}(a) \tag{A.1}$$

and

$$\int_0^1 x\mathrm{e}^{-ax} P_{2m+1}(x)\,\mathrm{d}x = \sqrt{\frac{2\pi}{a^3}}\left[\left(m+\frac{1}{2}\right) I_{2m+\frac{3}{2}}(a) + \left(\frac{a}{2}\right) I_{2m+\frac{5}{2}}(a)\right] - \frac{a\sqrt{\pi}}{4}\frac{{}_1F_2(\{2\},\{\frac{3}{2}-m,3+m\},\frac{a^2}{4})}{\Gamma(\frac{3}{2}-m)\Gamma(3+m)}. \tag{A.2}$$

These two expressions were derived with one of the definite integrals from [35]. Here, ${}_1F_2$ is the Barnes extended hypergeometric function, given by the series

$$\frac{{}_1F_2(\{a_1\},\{b_1,b_2\},x)}{\Gamma(b_2)\Gamma(b_1)} = \frac{1}{\Gamma(a_1)}\sum_{k=0}^{\infty}\frac{\Gamma(a_1+k)\,x^k}{\Gamma(b_1+k)\Gamma(b_2+k)\Gamma(k+1)}. \tag{A.3}$$

Straightforward numerical subroutines are available to compute the functions I_ν, K_ν, and ${}_1F_2$ [36, 37]. As the harmonic number m increases, the contributions to $\mathbf{f}_m$ from the modified Bessel functions decrease dramatically relative to those from ${}_1F_2$.

An analytical form for the integral of the Legendre polynomial in $\mathbf{g}_m$ is given by the relation [38]

$$\int_0^1 P_{2m+1}(x)\,\mathrm{d}x = \frac{(-1)^m\Gamma(m+\frac{1}{2})}{2\sqrt{\pi}\Gamma(m+2)}. \tag{A.4}$$

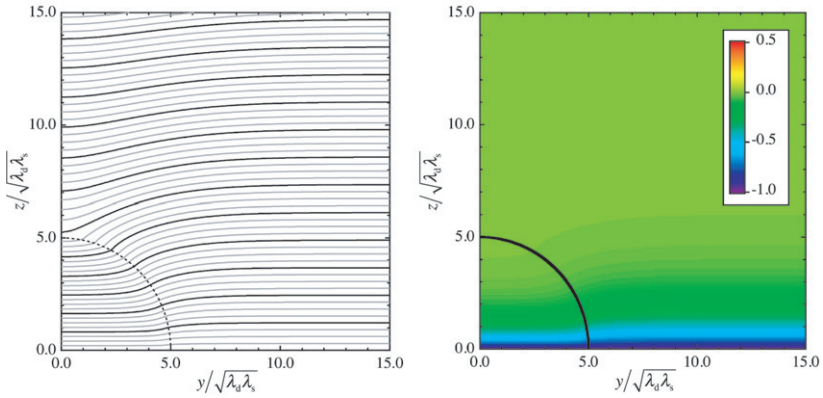

Figure B.1. Charge and potential distributions for $\delta = 5$ with $\phi^* = 0$. The droplet carries an unphysical net charge.

Equations (A.1), (A.2), and (A.4) give all the quantities needed to evaluate the Fourier–Legendre coefficients in equation (22).

Finally, an analytical expression is available for the integral contained in h_m. One can use

$$h_m = (\delta\zeta)^3 \left(\frac{\delta\zeta}{2}\right)^{2m+\frac{3}{2}} \frac{(-1)^m\, {}_1F_2(\{2+m\},\{m+3,2m+\frac{5}{2}\},\frac{\delta^2\zeta^2}{4})\Gamma(m+\frac{1}{2})}{4\sqrt{\pi}\Gamma(m+3)\Gamma(2m+\frac{5}{2})I_{2m+\frac{3}{2}}(\delta\zeta)} \tag{A.5}$$

to evaluate equation (24). Numerical accuracy is lost in this expression when $\delta\zeta$ is large.

Appendix B. The case of a permeable boundary

The charge-conservation equation (1) can be 'turned off' by setting ϕ^* to zero. Figure B.1 demonstrates the system response when typical PB electrostatics is employed and ions reflected from the liquid–liquid interface are ignored (the typical approach when droplets are large). In the figure, the potential decay looks like Debye screening from a planar electrode both within and outside the droplet. In addition, the potential plateaus visible in figure 3 have disappeared. There is no countercharge at the liquid–liquid surface, and there is a negative net charge on the droplet: thus, if the potential shift due to an impermeable liquid–liquid surface is neglected, the electrostatics yield an aphysical net charge on the droplet. This physical picture would be correct if the droplet had a permeable boundary.

Appendix C. Asymptotic expansions

C.1. Modified Bessel functions

Many of the quantities introduced in section 3.5 contain ratios of modified Bessel functions. In particular, it is necessary to expand the ratios of modified Bessel functions in $\mathbf{C}_m$ and h_m such that the lower-order corrections in δ are independent of m. This can be achieved with two of the expansions from [39]. For ratios of the form $I_{p+n}(x)/I_p(x)$, we define $\hat{I}_m^{(i)}(x,n)$ as the term of order x^{-i} in the ratio with $p = 2m + \frac{3}{2}$, such that

$$\frac{I_{2m+\frac{3}{2}+n}(x)}{I_{2m+\frac{3}{2}}(x)} \approx \hat{I}_m^{(0)}(x,n) - \frac{\hat{I}_m^{(1)}(x,n)}{x} - \frac{\hat{I}_m^{(2)}(x,n)}{x^2} + \mathrm{o}(x^{-3}). \tag{C.1}$$

Using expansion 7.13.2 (9) from [39], we find

$$\begin{aligned}
\hat{I}_m^{(0)}(x,n) &= A_{2m+\frac{3}{2},n}(x),\\
\hat{I}_m^{(1)}(x,n) &= A_{2m+\frac{3}{2},n}(x)\left[F\left(\frac{4m+3+2n}{2x}\right)-F\left(\frac{4m+3}{2x}\right)\right],\\
\hat{I}_m^{(2)}(x,n) &= A_{2m+\frac{3}{2},n}(x)\left[G\left(\frac{4m+3}{2x}\right)-G\left(\frac{4m+3+2n}{2x}\right)\right.\\
&\quad\left.+F\left(\frac{4m+3}{2x}\right)F\left(\frac{4m+3+2n}{2x}\right)\right].
\end{aligned}\tag{C.2}$$

The three functions introduced here are defined as

$$A_{p,n}(x)=\frac{\left[1+(\frac{p}{x})^2\right]^{\frac{1}{4}}\left[\frac{p}{x}+\sqrt{(\frac{p}{x})^2+1}\right]^p \mathrm{e}^{x\left[\sqrt{1+(\frac{p+n}{x})^2}-\sqrt{1+(\frac{p}{x})^2}\right]}}{\left[1+(\frac{p+n}{x})^2\right]^{\frac{1}{4}}\left[\frac{p+n}{x}+\sqrt{(\frac{p+n}{x})^2+1}\right]^{p+n}},\tag{C.3}$$

$$F(x)=-\frac{1}{8\sqrt{1+x^2}}\left[1-\frac{5x^2}{3\left(1+x^2\right)}\right],\tag{C.4}$$

$$G(x)=\frac{9}{128\left(1+x^2\right)}-\frac{231x^2}{576\left(1+x^2\right)^2}+\frac{1155x^4}{3456\left(1+x^2\right)^3}.\tag{C.5}$$

Ratios of the form $K_p(x)/K_{p+n}(x)$ can be treated in a similar fashion using expansion 7.13.2 (10) from [39]. Define $\hat{K}_m^{(i)}(x,n)$ as the term of order x^{-i} in the ratio with $p=2m+\frac{1}{2}$, such that

$$\frac{K_{2m+\frac{1}{2}}(x)}{K_{2m+\frac{1}{2}+n}(x)}=\hat{K}_m^{(0)}(x,n)-\frac{\hat{K}_m^{(1)}(x,n)}{x}-\frac{\hat{K}_m^{(2)}(x,n)}{x^2}+\mathrm{o}(x^{-3}).\tag{C.6}$$

Use of the asymptotic expansion shows that

$$\begin{aligned}
\hat{K}_m^{(0)}(x,n) &= B_{2m+\frac{1}{2},n}(x),\\
\hat{K}_m^{(1)}(x,n) &= B_{2m+\frac{1}{2},n}(x)\left[F\left(\frac{4m+1+2n}{2x}\right)-F\left(\frac{4m+1}{2x}\right)\right],\\
\hat{K}_m^{(2)}(x,n) &= B_{2m+\frac{1}{2},n}(x)\left[G\left(\frac{4m+1+2n}{2x}\right)-G\left(\frac{4m+1}{2x}\right)\right.\\
&\quad\left.+F\left(\frac{4m+1}{2x}\right)F\left(\frac{4m+1+2n}{2x}\right)\right],
\end{aligned}\tag{C.7}$$

where $F(x)$ and $G(x)$ are defined by equations (C.4) and (C.5), respectively, and

$$B_{p,n}(x)=\frac{\left[1+(\frac{p+n}{x})^2\right]^{\frac{1}{4}}\left[\frac{p}{x}+\sqrt{1+(\frac{p}{x})^2}\right]^p \mathrm{e}^{x\left[\sqrt{1+(\frac{p+n}{x})^2}-\sqrt{1+(\frac{p}{x})^2}\right]}}{\left[1+(\frac{p}{x})^2\right]^{\frac{1}{4}}\left[\frac{p+n}{x}+\sqrt{1+(\frac{p+n}{x})^2}\right]^{p+n}}\tag{C.8}$$

defines the function $B_{p,n}(x)$.

The functions $\hat{I}_m^{(i)}$ and $\hat{K}_m^{(i)}$ take into account the order dependence of the ratios, and are all $\mathrm{o}(\delta^0)$. Also, the ratios are defined such that, when x is fixed, both tend to zero as $p\to\infty$ or $n\to\infty$. In the limit as $x\to\infty$, both zero-order contributions to the ratios go to unity, and all corrections of order lower than zero go to zero.

C.2. Integrals in the Fourier–Legendre expressions

The precise forms of the asymptotic corrections given in equation (25) are

$$\mathbf{f}_m \approx \frac{(-1)^m\,\Gamma\,(2m+3)}{2^{2m}\Gamma\,(m+1)\,\Gamma(m+2)}\begin{bmatrix}\frac{1/\zeta^2-\zeta^2}{\delta^2}\\ 0\end{bmatrix}+\mathrm{o}(\delta^{-3}), \tag{C.9}$$

$$\mathbf{g}_m \approx \frac{(-1)^m\,\Gamma(m+\frac{1}{2})}{2\sqrt{\pi}\Gamma(m+2)}\begin{bmatrix}1\\ 0\end{bmatrix}+\frac{(-1)^{m+1}\,\Gamma\,(2m+3)}{\Gamma\,(m+1)\,\Gamma(m+2)2^{2m+1}}\begin{bmatrix}\frac{1}{(\delta\zeta)^2}\\ 0\end{bmatrix}+\mathrm{o}(\delta^{-3}). \tag{C.10}$$

Definitions (C.1) and (C.6) may be used to express $\mathbf{C}_m$ as

$$\mathbf{C}_m \approx \begin{bmatrix}-1 & 1\\ \frac{\zeta}{\chi}\hat{I}_m^{(0)}\,(\delta\zeta,1) & \frac{\chi}{\zeta}\hat{K}_m^{(0)}\,(\delta/\zeta,1)\end{bmatrix}+\begin{bmatrix}0 & 0\\ \frac{2m+1-\hat{I}_m^{(1)}(\delta\zeta,1)}{\delta\chi} & \frac{\chi\left[2(m+1)-\hat{K}_m^{(1)}(\delta/\zeta,1)\right]}{\delta}\end{bmatrix}$$
$$-\begin{bmatrix}0 & 0\\ \frac{\hat{I}_m^{(2)}(\delta\zeta,1)}{\delta^2\chi\zeta} & \frac{\chi\zeta\hat{K}_m^{(2)}(\delta/\zeta,1)}{\delta^2}\end{bmatrix}+\mathrm{o}(\delta^{-3}). \tag{C.11}$$

The last quantity containing ratios of Bessel functions is the integral over droplet volume in h_m. This expansion requires additional analysis. To obtain an asymptotic expression valid at large δ, one can use a derivative relation for the modified Bessel functions [40] and integrate successively by parts to show that

$$\int_0^\delta \xi^{\frac{3}{2}} I_{2m+\frac{3}{2}}\,(\xi\zeta)\;\mathrm{d}\xi = \frac{\Gamma\,(m+1)}{\Gamma\,(2m+1)\,\zeta^{\frac{5}{2}}}\sum_{k=0}^{\infty}\frac{\Gamma\,(2m+2k)\,(\delta\zeta)^{\frac{3}{2}-k}}{2^{k-1}\Gamma\,(m+k)}I_{2m+\frac{5}{2}+k}\,(\delta\zeta). \tag{C.12}$$

Insertion of this relation and equation (A.4) into equation (23) gives

$$h_m = \frac{(\delta\zeta)^2\,(-1)^m}{2\sqrt{\pi}\Gamma(m+2)}\sum_{k=0}^{\infty}\frac{\Gamma(m+k+\frac{1}{2})}{(\delta\zeta/2)^k}\frac{I_{2m+\frac{3}{2}+(k+1)}\,(\delta\zeta)}{I_{2m+\frac{3}{2}}\,(\delta\zeta)}, \tag{C.13}$$

which contains an infinite series of the ratios defined in equation (C.1). Inserting that expression demonstrates that

$$h_m \approx \frac{(\delta\zeta)^2\,(-1)^m}{2\sqrt{\pi}\Gamma(m+2)}\left[\sum_{k=0}^{\infty}\sum_{i=0}^{2}\frac{\Gamma(m+k+\frac{1}{2})\hat{I}_m^{(i)}\,(\delta\zeta,k+1)}{(\delta\zeta/2)^k}+\mathrm{o}(\delta^{-3})\right], \tag{C.14}$$

which are the higher-order corrections to h_m given in equation (27). All of the ratios go as $A_{2m+\frac{3}{2},k+1}\,(\delta\zeta)$; by substituting that function into equation (C.14), it can be verified that the sums over k are convergent when $\delta\zeta \geqslant 2$.

Appendix D. The three-phase contact region: potential and energetics

D.1. Potential distribution

Here we provide the potential distribution in the singular region near the line of three-phase contact and demonstrate that the energetic contribution of this region can be neglected in cases when droplets are large. Figure D.1 shows a coordinate system suitable to treat the contour along which the three phases meet. The region can be approximated as a wedge geometry, amenable to cylindrical coordinates. Let the axis of the cylinder be along the contact line, R denote a radial coordinate extending from the contact line, and Θ give the azimuthal angle of the cylinder, which ranges from 0 at the electrode in region d to π at the electrode in region s. With coordinates constructed in this fashion, α_c retains the same definition. The dimensionless radial coordinate, ρ, is given by

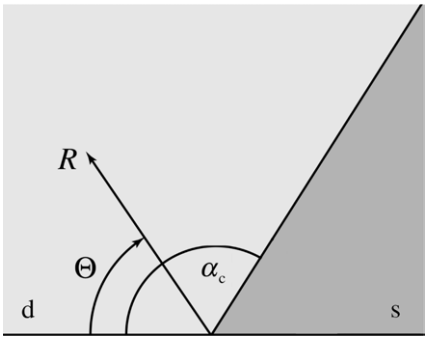

Figure D.1. Coordinate system for the region near the three-phase contact line.

$$\rho = \frac{R}{\sqrt{\lambda_d \lambda_s}}. \tag{D.1}$$

This region is taken to extend to radius ρ_0 around the three-phase contact line.

Because regions d and s are both semi-infinite in this case, the mass-conservation condition does not apply and the linearization around ϕ^* may be neglected in the formulation of the governing equations. The PB equations in the wedge geometry are

$$\begin{aligned} &\frac{\partial^2 \phi_d^{cl}}{\partial \rho^2} + \frac{1}{\rho}\frac{\partial \phi_d^{cl}}{\partial \rho} + \frac{1}{\rho^2}\frac{\partial^2 \phi_d^{cl}}{\partial \Theta^2} - \zeta^2 \phi_d^{cl} = 0, \qquad 0 \leqslant \Theta \leqslant \alpha_c, \\ &\frac{\partial^2 \phi_s^{cl}}{\partial \rho^2} + \frac{1}{\rho}\frac{\partial \phi_s^{cl}}{\partial \rho} + \frac{1}{\rho^2}\frac{\partial^2 \phi_s^{cl}}{\partial \Theta^2} - \frac{\phi_s^{cl}}{\zeta^2} = 0, \qquad \alpha_c \leqslant \Theta \leqslant \pi, \end{aligned} \tag{D.2}$$

where a superscript cl indicates the portion of the potential distribution owing to the region of three-phase contact. These equations take the boundary conditions

$$\phi_d^{cl}(\rho, 0) = 1, \qquad \phi_s^{cl}(\rho, \pi) = 1, \tag{D.3}$$

and the matching conditions

$$\phi_d^{cl}(\rho, \alpha_c) = \phi_s^{cl}(\rho, \alpha_c), \qquad \frac{1}{\chi}\left.\frac{\partial \phi_d^{cl}}{\partial \Theta}\right|_{(\rho,\alpha_c)} = \chi \left.\frac{\partial \phi_s^{cl}}{\partial \Theta}\right|_{(\rho,\alpha_c)}. \tag{D.4}$$

Using superposition to account for the typical solution for potential around a semi-infinite isopotential surface, the problem can be solved with distributions

$$\begin{aligned} \phi_d^{cl}(\rho, \Theta) &= e^{-\rho\zeta \sin\Theta} + \varphi_d^{cl}, \\ \phi_s^{cl}(\rho, \Theta) &= e^{-\rho \sin\Theta/\zeta} + \varphi_s^{cl}. \end{aligned} \tag{D.5}$$

The resulting equations for φ_j^{cl} are homogeneous and separable.

To obtain the unknown functions φ_j^{cl}, it is most direct to use the Kontorovich–Lebedev integral transformation [41]. The forward and inverse Kontorovich–Lebedev transformations are defined as

$$\begin{aligned} \mathcal{L}_\nu\{f(\rho)\} &\equiv \frac{2}{\pi^2}\int_0^\infty f(\rho)\, K_{iw}(\nu\rho)\, \frac{d\rho}{\rho} = \overline{f}(w), \\ \mathcal{L}_\nu^{-1}\left\{\overline{f}(w)\right\} &\equiv \int_0^\infty \overline{f}(w) w K_{iw}(\nu\rho) \sinh(\pi w)\, dw = f(\rho), \end{aligned} \tag{D.6}$$

where $\mathcal{L}_\nu\{\,\}$ denotes the Kontorovich–Lebedev operator and an overbar indicates a transformed function.

As the goal here is to illustrate qualitative behaviour of the potential in the singular region, we take $\zeta = 1$ to simplify the problem. Then $\nu = 1$ in the transformation for regions d and s. Corrections to normal Debye screening for the potential distributions are given by

$$\begin{aligned}\varphi_{\mathrm{d}}^{\mathrm{cl}}(\rho,\Theta) &= \mathcal{L}_1^{-1}\left\{\overline{R}_{\mathrm{d}}(w)\sinh(w\Theta)\right\},\\ \varphi_{\mathrm{s}}^{\mathrm{cl}}(\rho,\Theta) &= \mathcal{L}_1^{-1}\left\{\overline{R}_{\mathrm{s}}(w)\sinh[w(\pi-\Theta)]\right\}.\end{aligned} \tag{D.7}$$

The functions $\overline{R}_{\mathrm{d}}$ and $\overline{R}_{\mathrm{s}}$ give the radial dependence of the potentials in the frequency domain. They can be obtained from the transformations of the potential- and electric displacement-matching conditions, which result in the expressions

$$\begin{aligned}\overline{R}_{\mathrm{d}}(w) &= \frac{\pi\left(1-\chi^2\right)\sinh\left[w\left(\frac{\pi}{2}-\alpha_{\mathrm{c}}\right)\right][w(\pi-\Theta)]}{wb(w)\sinh(\pi w)},\\ \overline{R}_{\mathrm{s}}(w) &= \frac{\pi\left(1-\chi^2\right)\sinh\left[w\left(\frac{\pi}{2}-\alpha_{\mathrm{c}}\right)\right]\sinh(w\alpha_{\mathrm{c}})}{wb(w)\sinh(\pi w)},\end{aligned} \tag{D.8}$$

in which the function $b(w)$ is defined as

$$b(w) = \chi^2\cosh[w(\pi-\alpha_{\mathrm{c}})]\sinh(w\alpha_{\mathrm{c}}) + \sinh[w(\pi-\alpha_{\mathrm{c}})]\cosh(w\alpha_{\mathrm{c}}). \tag{D.9}$$

In addition, one can use the series expansion [42]

$$K_{\mathrm{i}w}(\rho) = \frac{\pi}{2\mathrm{i}\sinh\pi w}\sum_{k=0}^{\infty}\frac{(\rho/2)^{2k}}{\Gamma(k+1)}\left[\frac{(\rho/2)^{-\mathrm{i}w}}{\Gamma(k+1-\mathrm{i}w)} - \frac{(\rho/2)^{\mathrm{i}w}}{\Gamma(k+1+\mathrm{i}w)}\right] \tag{D.10}$$

to express the modified Bessel functions. After inserting this expansion, a change of variables allows the inverse Kontorovich–Lebedev transformations to be expressed as

$$\begin{aligned}\frac{\mathrm{i}\varphi_{\mathrm{d}}^{\mathrm{cl}}(\rho,\Theta)}{1-\chi^2} &= \sum_{k=0}^{\infty}\int_{-\infty}^{\infty}\frac{\sinh[w(\pi-\alpha_{\mathrm{c}})]\sinh\left[\left(\frac{\pi}{2}-\alpha_{\mathrm{c}}\right)w\right]\sinh(w\Theta)}{b(w)\sinh(\pi w)\Gamma(k+1)\Gamma(k+1-\mathrm{i}w)}\left(\frac{\rho}{2}\right)^{2k-\mathrm{i}w}\mathrm{d}w,\\ \frac{\mathrm{i}\varphi_{\mathrm{s}}^{\mathrm{cl}}(\rho,\Theta)}{1-\chi^2} &= \sum_{k=0}^{\infty}\int_{-\infty}^{\infty}\frac{\sinh(w\alpha_{\mathrm{c}})\sinh\left[\left(\frac{\pi}{2}-\alpha_{\mathrm{c}}\right)w\right]\sinh[w(\pi-\Theta)]}{b(w)\sinh(\pi w)\Gamma(k+1)\Gamma(k+1-\mathrm{i}w)}\left(\frac{\rho}{2}\right)^{2k-\mathrm{i}w}\mathrm{d}w.\end{aligned} \tag{D.11}$$

Equation (D.9) for $b(w)$ shows that the integrand of the inversion integral has poles along the imaginary axis. The locations of the poles can be obtained from the roots of

$$\chi^2\tan\left(w_{\mathrm{p}}\alpha_{\mathrm{c}}\right) + \tan\left[w_{\mathrm{p}}(\pi-\alpha_{\mathrm{c}})\right] = 0, \tag{D.12}$$

where w_{p} denotes a pole. Note that w_{p} takes a real value (the poles are along the imaginary axis at $\mathrm{i}w_{\mathrm{p}}$), and that $w_{\mathrm{p}} = 0$ is not a pole because of the forms of the numerators in equations (D.11). The pole closest to zero in the upper half-plane, denoted w_0, dominates the inversion integral.

Examination of the denominators in equations (D.11) shows that no branch cuts are necessary. The corrections to the potentials for $0 \leqslant \rho < \rho_0$ are therefore given by the theorem of residues, which yields

$$\begin{aligned}\varphi_{\mathrm{d}}^{\mathrm{cl}}(\rho,\Theta) &= M_0(\alpha_{\mathrm{c}},\chi)\sin[w_0(\pi-\alpha_{\mathrm{c}})]\sin(w_0\Theta)\,I_{w_0}(\rho),\\ \varphi_{\mathrm{s}}^{\mathrm{cl}}(\rho,\Theta) &= M_0(\alpha_{\mathrm{c}},\chi)\sin(w_0\alpha_{\mathrm{c}})\sin[w_0(\pi-\Theta)]\,I_{w_0}(\rho),\end{aligned} \tag{D.13}$$

in which the function M_0 is defined as

$$\begin{aligned}M_0(\alpha_{\mathrm{c}},\chi) = {}& \frac{2\pi\left(\chi^2-1\right)\sin\left[w_0\left(\frac{\pi}{2}-\alpha_{\mathrm{c}}\right)\right]}{\sin(\pi w_0)}\\ &\times\left\{\left[(\pi-\alpha_{\mathrm{c}})+\chi^2\alpha_{\mathrm{c}}\right]\cos(w_0\alpha_{\mathrm{c}})\cos[w_0(\pi-\alpha_{\mathrm{c}})]\right.\\ &\left.-\left[\chi^2(\pi-\alpha_{\mathrm{c}})+\alpha_{\mathrm{c}}\right]\sin(w_0\alpha_{\mathrm{c}})\sin[w_0(\pi-\alpha_{\mathrm{c}})]\right\}^{-1},\end{aligned} \tag{D.14}$$

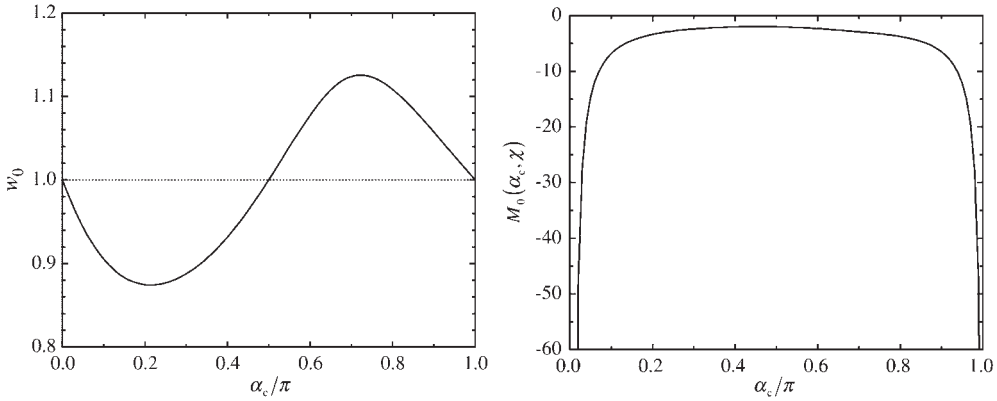

Figure D.2. Plots of w_0 and M_0 as a function of α_c for $\chi = 1.5$ and $\zeta = 1$.

and the value of w_0 is given by the first positive (nonzero) root of equation (D.12). The value of ρ_0, which gives the size of this region, was estimated to be 0.1 Debye lengths, as suggested by the value of θ_{zc} from the asymptotics for hemispheres at $\delta\zeta = 1225$.

Figure D.2 presents w_0 and M_0 as functions of α_c for the value of χ given in table 1. From the figure, one can see that w_0 is near unity for all contact angles. When the contact angle is obtuse, $w_0 > 1$, showing that the fields converge at the three-phase contact line (as $\rho \to 0$). The fields diverge when contact angles are acute. The opposite behaviour holds when $\chi < 1$. When $\chi = 1$, w_0 is uniformly equal to 1. Because $w_0 > 0.5$ in all of these cases, the electrostatic energy of the three-phase contact line converges, although the fields diverge.

The plot of $M_0(\alpha_c, \chi)$ in figure D.2 shows that it is always negative; typical Debye screening is enhanced along the three-phase contact line for all contact angles. This behaviour holds at all magnitudes of χ. Although M_0 diverges as contact angles approach 0 or π, the additional sine functions in equations (D.13) cause φ_d^{cl} and φ_s^{cl} to go to zero at these extremes.

D.2. Neglect of the three-phase contact region for large droplets

To determine the impact of the three-phase contact line when droplets are large, one can compare the work to polarize regions ds and de under the large-droplet approximation to the work required to polarize the region near the three-phase contact line where the potential changes along the liquid–liquid surface.

Our analysis of the potential distribution was simplified by taking $\zeta = 1$. The energy contribution of this region relative to the reference state, $\Delta\mathscr{E}_{cl}$, can be expressed as

$$\frac{\Delta\mathscr{E}_{cl}}{2\pi\epsilon_0\Phi_0^2\sqrt{\lambda_d\lambda_s\epsilon_d\epsilon_s}} = N(\alpha_c, \chi)\frac{\delta\sqrt{\eta - 1}}{\eta} \tag{D.15}$$

when ζ is unity. This is the energy to polarize a region with radius $0.1\sqrt{\lambda_d\lambda_s}$ around the line of three-phase contact (a range suggested by the hemispherical solution for x_{zc} at $\delta\zeta = 1225$), and is taken relative to a droplet-free reference state.

The function $N(\alpha_c, \chi)$ relies on quantities arising from the integration in equation (42). N is plotted with respect to contact angle in figure D.3. Equations (44) and (D.15) show that $\Delta\mathscr{E}$ is of order δ^2 and $\Delta\mathscr{E}_{cl}$ is of order δ. Thus, the ratio $\Delta\mathscr{E}_{cl}/\Delta\mathscr{E}$ is proportional to $1/\delta$; as the droplet volume increases, the contribution of the three-phase contact region to the total energy shrinks as $V_d^{-1/3}$.

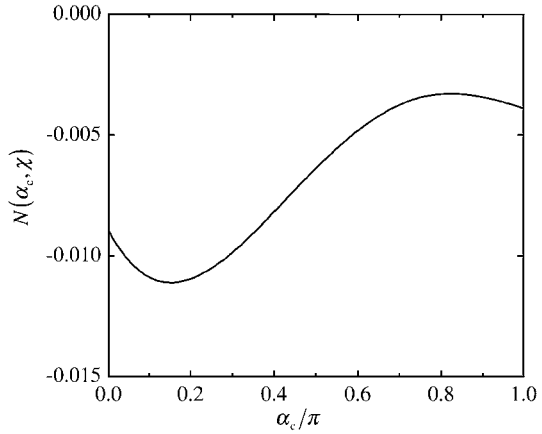

Figure D.3. Plot of $N(\alpha_c, \chi)$ as a function of α_c for $\chi = 1.5$ and $\zeta = 1$.

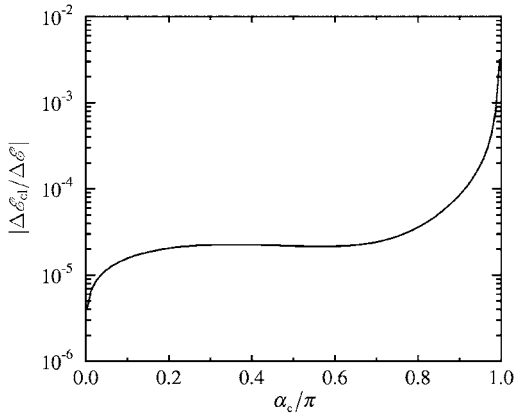

Figure D.4. Plot of $|\Delta\mathscr{E}_{cl}/\Delta\mathscr{E}|$ as a function of α_c for droplets of constant volume with $\chi = 1.5$ and $\zeta = 1$. The value of δ is 1225 at $\alpha_c = \pi/2$.

Figure D.4 shows the electrostatic energy of the three-phase contact region in comparison to those of the two-phase interfaces as a function of contact angle. The presented data are for droplets with $\zeta = 1$ and $\chi = 1.5$; the volume is set to that of a hemispherical droplet with $\delta = 1225$. This value of δ is the lower limit of validity of the approximation that $\delta \to \infty$ for hemispherical droplets, and thus is the upper bound of $|\Delta\mathscr{E}_{cl}/\Delta\mathscr{E}|$ in the large-droplet approximation. The figure demonstrates that the contribution of the three-phase contact line is less than 1% of $\Delta\mathscr{E}$ at all contact angles, and is in fact less than 0.01% of it when α_c is less than $8\pi/9$ (160°). This concludes the demonstration that for large droplets—that is, for droplets with $V_d \gg 2\pi(1225\lambda_d)^3/3$—one can neglect the three-phase contact line and use the large-droplet approximation to describe electrostatic contributions to the free energy.

For the electrostatic contribution of the three-phase contact line, $\Delta\mathscr{E}_{cl}$, to be neglected when minimizing the total free energy (as in section 5), its derivative with respect to contact angle must be small compared to the derivative with respect to contact angle of $\Delta\mathscr{E}$. A comparison of these derivatives shows that the change in $\Delta\mathscr{E}_{cl}$ is less than 1% of the change in $\Delta\mathscr{E}$ at all contact angles when $\delta\zeta = 1225$, justifying its neglect.

References

[1] Berge B and Peseux J 2000 Variable focal lens controlled by an external voltage: an application of electrowetting *Eur. Phys. J.* E **3** 159

[2] Kuiper S and Hendriks B H W 2004 Variable-focus liquid lens for miniature cameras *Appl. Phys. Lett.* **85** 1128

[3] Hayes R A and Feenstra B J 2003 Video-speed electronic paper based on electrowetting *Nature* **425** 383

[4] Beni G and Tenan M A 1981 Dynamics of electrowetting displays *J. Appl. Phys.* **52** 6011

[5] Beni G, Hackwood S and Jackel J L 1982 Continuous electro-wetting effect *Appl. Phys. Lett.* **40** 912

[6] Jackel J L, Hackwood S, Veselka J J and Beni G 1983 Electrowetting switch for multimode optical fibers *Appl. Opt.* **22** 1765

[7] Lee J and Kim C J 2000 Surface-tension-driven microactuation based on continuous electrowetting *J. Microelectromech. Syst.* **9** 171

[8] Yun K S, Cho I J, Bu J U, Kim C J and Yoon E 2002 A surface-tension micropump for low-voltage and low-power operations *J. Microelectromech. Syst.* **11** 454

[9] Gavach C, Seta P and d'Epenoux B 1977 The double layer and ion adsorption at the interface between two non miscible solutions part I. Interfacial tension measurements for the water-nitrobenzene tetraalkylammonium bromide systems *J. Electroanal. Chem.* **83** 225

[10] Kakiuchi T and Senda M 1983 Polarizability and electrocapillary measurements of the nitrobenzene water interface *Bull. Chem. Soc. Japan* **56** 1322

[11] Samec Z, Homolka D, Mareček V and Kavan L 1983 Charge transfer between two immiscible electrolyte solutions *J. Electroanal. Chem.* **145** 213

[12] Girault H H and Schiffrin D J 1985 Electrochemistry of liquid–liquid interfaces *Electroanalytical Chemistry* vol 15, ed A J Bard (New York: Dekker)

[13] Volkov A G, Deamer D W, Tanelian D L and Markin V S 1996 Electrical double layers at the oil/water interface *Prog. Surf. Sci.* **53** 1

[14] Benjamin I 1997 Molecular structure and dynamics at liquid–liquid interfaces *Annu. Rev. Phys. Chem.* **48** 407

[15] Schmickler W 2000 A lattice-gas model for ion pairing at liquid–liquid interfaces *J. Electroanal. Chem.* **483** 18

[16] Daikhin L I, Kornyshev A A and Urbakh M 2001 Ion penetration into an 'unfriendly medium' and the double layer capacitance of the interface between two immiscible electrolytes *J. Electroanal. Chem.* **500** 461

[17] Monroe C W, Urbakh M and Kornyshev A A 2005 Understanding the anatomy of capacitance at interfaces between two immiscible electrolytic solutions *J. Electroanal. Chem.* **582** 28

[18] Tasakorn P, Chen J Y and Aoki K 2002 Voltammetry of a single oil droplet on a large electrode *J. Electroanal. Chem.* **533** 119

[19] Davies T J, Evans R G, Hignett G, Wain A J, Lawrence N S, Wadhawan J D, Marken F and Compton R G 2003 Electrochemistry of immobilised redox droplets: concepts and applications *Phys. Chem. Chem. Phys.* **5** 4053

[20] Marken F 2004 Electrifying interfaces *Phil. Trans. R. Soc.* A **362** 2611

[21] Chou T 2001 Geometry-dependent electrostatics near contact lines *Phys. Rev. Lett.* **87** 106101

[22] Buehrle J, Herminghaus S and Mugele F 2003 Interface profiles near three-phase contact lines in electric fields *Phys. Rev. Lett.* **91** 086101

[23] Mugele F and Baret J-C 2005 Electrowetting: from basics to applications *J. Phys.: Condens. Matter* **17** R705

[24] Papathanasiou A G and Boudouvis A G 2005 Manifestation of the connection between dielectric breakdown strength and contact angle saturation *Appl. Phys. Lett.* **86** 164102

[25] Weast R C (ed) 1978 *CRC Handbook of Chemistry and Physics* 59th edn (West Palm Beach, FL: CRC Press) p E61

[26] Whittaker E T and Watson G N 1962 *A Course of Modern Analysis* 4th edn (Cambridge: Cambridge University Press) p 303

[27] Yoshida J, Chen J and Aoki K 2003 Electrochemical coalescence of nitrobenzene/water emulsions *J. Electroanal. Chem.* **553** 117

[28] Verwey E J W and Niessen K F 1939 The electrical double layer at the interface of two liquids *Phil. Mag.* **28** 435

[29] Landau L D, Lifshitz E M and Pitaevskii L P 2000 *Electrodynamics of Continuous Media* 2nd edn (Oxford: Butterworth-Heinemann) p 46

[30] Safran S A 1994 *Statistical Thermodynamics of Surfaces, Interfaces and Membranes* (Reading, MA: Addison-Wesley)

[31] Markin V S, Volkov A G and Volkova-Gugeshashvili M I 2005 Structure of nonpolarizable water/nitrobenzene interface: potential distribution, ion adsorption, and interfacial tension *J. Phys. Chem.* B **109** 16444

[32] Vallet M, Vallade M and Berge B 1999 Limiting phenomena for the spreading of water on polymer films by electrowetting *Eur. Phys. J.* B **11** 583

[33] Starks C, Liotta C and Halpern M 1994 *Phase-Transfer Catalysis: Fundamentals, Applications and Industrial Perspectives* (New York: Chapman and Hall)

[34] Volkov A G, Deamer D W, Tanelian D L and Markin V S 1998 *Liquid Interfaces in Chemistry and Biology* (New York: Wiley)
[35] Gradstein I S and Ryshik I M (ed) 1981 *Tables of Series, Integrals, and Products, German and English* vol 2 (Moscow: MIR) p 208
[36] Press W H, Teukolsky S A, Vetterling W T and Flannery B P (ed) 1992 *Numerical Recipes in Fortran 77* (Cambridge: Cambridge University Press) pp 239–43
[37] Moshier S L 2000 website. Search: 1F2, at http://www.codecogs.com/
[38] Hochstrasser U W 1972 Orthogonal polynomials *Handbook of Mathematical Functions* ninth printing, ed M A Abramowitz and I A Stegun (New York: Dover) p 786
[39] Bateman H and Erdélyi A 1953 *Higher Transcendental Functions* vol 2 (New York: McGraw-Hill) pp 99–100
[40] Dwight H B 1961 *Tables of Integrals and Other Mathematical Data* 4th edn (New York: Macmillan) p 189
[41] Kontorovich M J and Lebedev N N 1938 On a method of solving some problems of diffraction theory and related problems *Zh. Eksp. Teor. Fiz.* **8** 1192
[42] Gil A, Segura J and Temme N M 2003 Computation of the modified Bessel function of the third kind of imaginary orders: uniform airy-type asymptotic expansion *J. Comput. Appl. Math.* **153** 225